Measurement of the nucleation of atmospheric aerosol particles

Markku Kulmala[1], Tuukka Petäjä[1], Tuomo Nieminen[1], Mikko Sipilä[1], Hanna E Manninen[1], Katrianne Lehtipalo[1], Miikka Dal Maso[1], Pasi P Aalto[1], Heikki Junninen[1], Pauli Paasonen[1], Ilona Riipinen[2], Kari E J Lehtinen[3,4], Ari Laaksonen[4,5] & Veli-Matti Kerminen[1]

[1]Department of Physics, University of Helsinki, Helsinki, Finland. [2]Department of Applied Environmental Science & Bert Bolin Center for Climate Research, University of Stockholm, Stockholm, Sweden. [3]Kuopio Unit, Finnish Meteorological Institute, Kuopio, Finland. [4]Department of Physics and Mathematics, University of Eastern Finland, Kuopio, Finland. [5]Finnish Meteorological Institute, Helsinki, Finland. Correspondence should be addressed to M.K. (markku.kulmala@helsinki.fi).

Published online 16 August 2012; doi:10.1038/nprot.2012.091

The formation of new atmospheric aerosol particles and their subsequent growth have been observed frequently at various locations all over the world. The atmospheric nucleation rate (or formation rate) and growth rate (GR) are key parameters to characterize the phenomenon. Recent progress in measurement techniques enables us to measure atmospheric nucleation at the size (mobility diameter) of 1.5 (±0.4) nm. The detection limit has decreased from 3 to 1 nm within the past 10 years. In this protocol, we describe the procedures for identifying new-particle-formation (NPF) events, and for determining the nucleation, formation and growth rates during such events under atmospheric conditions. We describe the present instrumentation, best practices and other tools used to investigate atmospheric nucleation and NPF at a certain mobility diameter (1.5, 2.0 or 3.0 nm). The key instruments comprise devices capable of measuring the number concentration of the formed nanoparticles and their size, such as a suite of modern condensation particle counters (CPCs) and air ion spectrometers, and devices for characterizing the pre-existing particle number concentration distribution, such as a differential mobility particle sizer (DMPS). We also discuss the reliability of the methods used and requirements for proper measurements and data analysis. The time scale for realizing this procedure is 1 year.

INTRODUCTION

The formation of new atmospheric aerosol particles is a key phenomenon associated with the atmospheric aerosol system. Atmospheric aerosol formation consists of a complicated set of processes, including the production of nanometer-sized clusters from gaseous vapors, the growth of these clusters to detectable sizes and the removal of the growing clusters by coagulation with the pre-existing aerosol particle population[1]. Once formed, aerosol particles need to grow to sizes >50–100 nm in diameter before they are able to influence climate, although smaller particles may affect human health and atmospheric chemistry. The formation of new aerosol particles has been observed to take place almost everywhere in the atmosphere[2,3]. The pioneers in these observations were Weber *et al.*[4,5] and Mäkelä *et al.*[6]. There are substantial variations in the intensities and spatial scales of atmospheric NPF: it can be a large regional phenomenon

extending over a thousand kilometers[7,8] or it can occur in intensive bursts, e.g., on a coastline[9,10]. The total particle number concentration in regional background conditions, as well as in the global troposphere, is very likely to be dominated by NPF[11,12]. Particles formed in the atmosphere markedly affect the cloud condensation nuclei concentrations and thus indirectly affect Earth's radiative balance[3–15].

Atmospheric NPF events are usually characterized by two quantities: the particle formation rate and particle GR. The former quantity is the rate ($cm^{-3}\ s^{-1}$) at which new aerosol particles are being produced in the atmosphere, whereas the latter tells how rapidly they grow to larger sizes ($nm\ h^{-1}$). The measured NPF rate is usually not the atmospheric nucleation rate, but the rate at which particles appear into the smallest measurable sizes, typically a few nanometers in diameter. This size is quite often 3 nm; however, because of the recent improvements, particles of 2 nm in diameter or even smaller can be detected[16–18].

The longest continuous measurements to collect data for atmospheric NPF[19] are from the Station for Measuring Forest-Atmosphere Relations (SMEAR II) in Hyytiälä, Finland[20]. The recording of measurements started in January 1996 (ref. 6) and is still continuing. During these years, the size of the smallest particles that can be detected has decreased from 3.0 nm to 1.1 ($\pm$ 0.2) nm (**Fig. 1**). The size at which the formation rate has been determined has correspondingly decreased from 3 to 2 nm, and then even further down to 1.5 nm (refs. 4,16,21). Recently, in the CLOUD (Cosmics Leaving Outdoor Droplets) experiment at CERN, particles 1.7 nm in size have been used to determine the nucleation rate[22]. The present estimate of the size at which atmospheric nucleation occurs is 1.5 nm ($\pm$ 0.4 nm)[16,21,22].

Studying atmospheric aerosol formation requires measurements of both physical and chemical properties of nucleation-mode (<25 nm in diameter) particles, both charged and neutral, as well as the

whole ambient aerosol number size distribution. Simultaneous measurements of nucleating gases, or their proxies, provide further insights into nucleation mechanisms and particle growth processes[23–33]. Besides physical properties, it is also crucial to measure the chemical composition of nucleation-mode aerosol particles and to find out ways to determine the chemical composition of the growing clusters[34–37].

In this protocol, we will present the main methods to measure the size distribution and concentrations of nanoparticles, determine their formation (and/or nucleation) and subsequent growth rates, and recognize and delineate the periods of regional NPF events from a long time series. The main instruments and methods needed for these procedures will also be presented. We will focus on regional NPF events, in which NPF is occurring simultaneously over a large spatial scale[2,3]. Note that the methods presented here

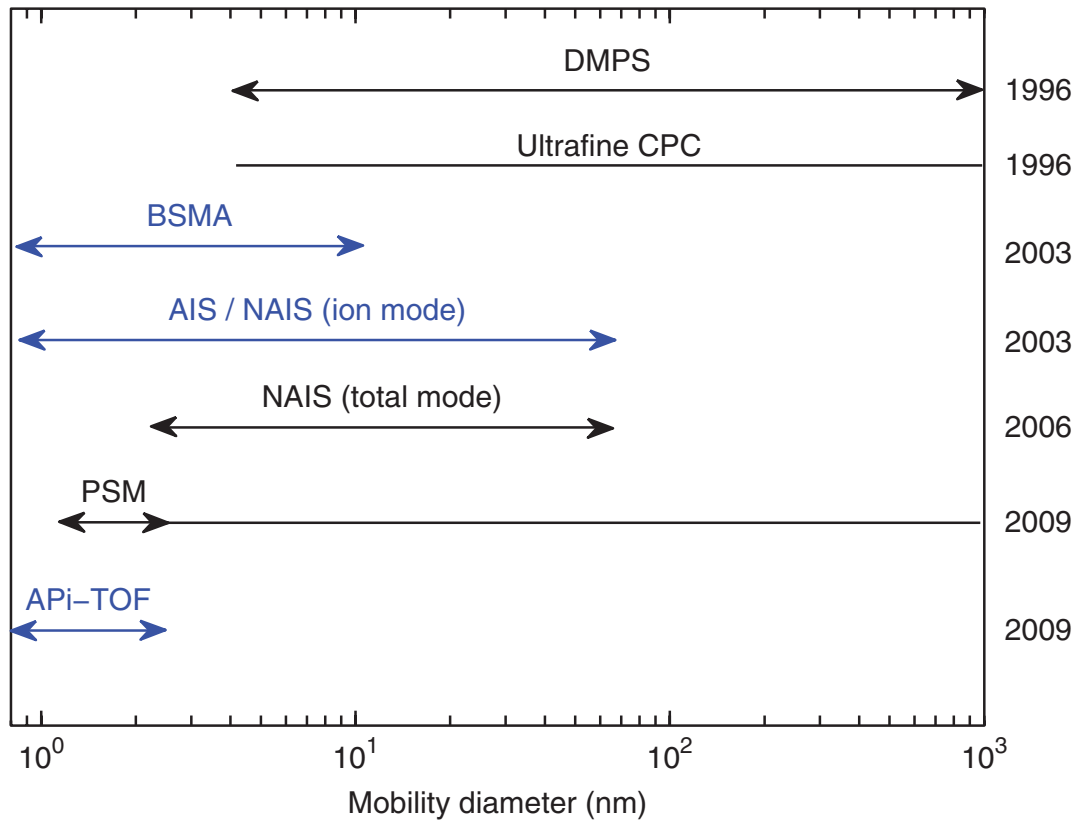

Figure 1 | The size ranges of different measurement techniques, organized by the development time of the instrument. The year when each was first applied at the SMEAR II station in Hyytiälä[18] is indicated on the right-hand side. The arrowheads indicate the region in which size distribution can be retrieved. Blue lines represent ion measurements, whereas black lines represent measurements of total particle population.

are the ones we use currently. As this field continuously evolves, the methods need to be updated and modified in the future.

Requirements for measuring nucleation of atmospheric aerosol particles

For this procedure, the primary measurement data set needed for determining the formation rate of particles is the aerosol particle number concentration as a function of time and particle size down to a few nanometers, preferably down to the size where the initial formation occurs (1.5 ± 0.4 nm). Here we first present the measurement techniques used and describe the considerations necessary for making the required measurements. After that, we present the NPF event analysis and the determination of particle GRs, which are the necessary steps in finally determining the atmospheric particle formation or nucleation rates.

The particle number size distribution is defined by the formation processes and subsequent physical and chemical processes in the atmosphere. The appropriate particle size definition depends primarily on the type of measurement made and on the physicochemical processes in question.

All size measurements discussed in this protocol are based on the particle electrical mobility, Z_p. In this protocol, the conversion between electrical mobility and electrical mobility diameter (d_p) is done according to an equation[38]:

$$Z_p = \frac{neC_c}{3\pi\eta d_p} \quad (1)$$

where n is number of excess elementary charges e carried by the particle, η is viscosity of air and C_c is the Cunningham slip correction factor given by a empirical equation[39]. A complete list of abbreviations and nomenclature can be found in **Table 1**.

The geometric diameter, which is related to particle mass and can be estimated from the particle bulk density, is about 0.3 nm smaller than the electrical mobility diameter[40–42]. As the diameter is not a well-defined concept at very small sizes or for highly nonspherical particles, we choose to use the electrical mobility diameter as it can be readily converted back to the particle electrical mobility, which is usually the measured quantity.

TABLE 1 | Abbreviations and nomenclature.

C_c	Cunningham slip correction factor
CoagS_{d_p}	Coagulation sink at size d_p
CS	Coagulation sink
D	Diffusion coefficient
d^*	Critical cluster size (i.e., the size at which nucleation occurs)
d_p	Electrical mobility equivalent diameter
$d_{p,cutoff}$	Cutoff size (i.e., the lower detection limit of the instrument measuring the particle concentration (e.g., CPC))
$dn/d\ (\log_{10}Z_p)$	Ion/particle mobility distribution
$dn/d\ (\log_{10}d_p)$	Ion/particle number size distribution
e	Elementary charge
GR	Growth rate
$\mathrm{GR}_{d^*-d_p}$	Growth rate from initial nucleation at d^* to size d_p
J_{d_p}	Formation rate at size d_p
$J_{d_p}{}^{\pm}$	Formation rate of positive or negative ions

J^*	Nucleation rate at size d^*
$K\ (d_p, d_p')$	Coagulation coefficient between particles of d_p and d_p' sizes
Kn	Knudsen number
m	Semiempirical coefficient for scaling CS and $CoagS_{dp}$
N_{dp}	Particle concentration at size d_p
$N_{dp}^{\pm}$	Ion/charged particle concentration at d_p
n	Number of elementary charges in particle
S_{losses}	Additional losses for particles
t	Time
Z_P	Ion/particle electrical mobility
α	Ion-ion recombination coefficient
β_m	Fuchs-Sutugin transition regime correction factor
λ	Mean free path
γ	Semiemprical parameter for scaling nucleation rate from observed formation rate
η	Viscosity of air
χ	Ion-aerosol attachment coefficient

The quantities that will be derived from the measurements are the formation rate of particles (J_{d_P}) at the diameter d_P (in nm) and the GR of nucleated particles at different size intervals. The following issues should be considered when selecting the instrumentation (required instruments given in parentheses):

- Detection of the number concentration (CPC[43–47]) and size distribution (DMPS[48–51] or scanning mobility particle sizer (SMPS)[52]) of small particles down to 2.5 nm in diameter (current typical detection limit) to obtain J_3.
- Detection of the number concentration (particle size magnifier (PSM)[18], CPC or condensation particle counter battery (CPCB)[53,54]) and size distribution (PSM, neutral cluster and air ion spectrometer (NAIS)[16,55], diethylene glycol (DEG)-SMPS[47] or pulse-height(PH)-CPC[56–60]) of particles <3 nm and clusters, preferably down to 1.1–1.5 nm in diameter, to obtain J_2 or $J_{1.5}$, which approximates the nucleation rate.
- Detection of the number concentration and size distribution of ions (i.e., charged particles and clusters), down to 0.5–1 nm in diameter (air ion spectrometer (AIS)[61,62], balanced scanning mobility analyzer (BSMA)[63], inclined grid mobility analyzer (IGMA) or symmetric inclined grid mobility analyzer (SIGMA)[64]), to obtain the formation rate of charged particles and ion-induced nucleation rate.
- Time resolution of about 10 min (DMPS, SMPS or DEG-SMPS) for ground-based or ship measurements, or from a fraction of a second up to 1 min (CPC, CPCB, PSM, PH-CPC or NAIS), for aircraft measurements, to obtain GRs and nucleation rates.
- Size resolution, involving multiple channels in the size range of <3 to 20 nm (NAIS or DEG-SMPS) or 3 to 20 nm (DMPS or SMPS) for neutral particles and in the range of 0.5 to 10 nm for ions (AIS, BSMA, IGMA or SIGMA), in order to detect the

possible growth of clusters and particles after nucleation to obtain GR.

- The ability to measure low-nucleation-mode concentrations (<500 cm^{-3}) found in clean and remote atmospheres (CPC, CPCB, PSM, PH-CPC, DMPS).
- The ability to measure high-nucleation-mode concentrations (>10^5 cm^{-3}) found during intense nucleation bursts occurring in coastal areas and heavily polluted environments (DMPS, SMPS, DEG-SMPS, CPC, CPCB, PSM, NAIS).
- The ability to determine the constraining parameters (pre-existing condensation sink (CS) both in submicron and supermicron ranges) and the environmental parameters that can affect this sink (hygroscopicity, ambient meteorological conditions).

The condensation technique is a commonly used methodology to determine aerosol particle concentration above a certain cutoff size. The working principle of a CPC (also sometimes called condensation nuclei counter) is that the aerosol sample is exposed to a supersaturated vapor, which condenses on the particles making them large enough to be observed optically. The continuous flow rate and fast response time make the modern CPCs suitable for field studies, and connectable to, for example, size spectrometers such as the DMPS/SMPS in order to yield a particle size spectrum. See the **Supplementary Methods** for details.

The lower limit of a CPC is described by its cutoff size. The cutoff size is defined as the lowest particle diameter at which the instrument detects at least half of the particles. The cutoff diameter and the steepness of the cutoff curve are determined both by the

activation probability of particles (which in turn depends both on the created supersaturation profile in the instrument and the

physicochemical properties of the particles), and by diffusion losses of particles inside the instrument. The first CPCs designed specifically for ultrafine particles (ultrafine CPCs) were developed in the 1990s (ref. 43), and had a cutoff size of about 3 nm, which remained the lowest detectable size for a long time. In the recent years, cutoff sizes down to 1 nm have been obtained using, e.g., DEG as the working fluid[17,18,46,47]. A side-by-side operation of CPCs with a variable cutoff size and/or working fluid will provide insights into rapid changes of number concentration and chemical composition of the nanoparticles[53].

The CPC is able to detect both neutral and charged particles without a need to neutralize the particle population, and without the additional diffusion losses of a size-selection unit. In addition, the signal-to-noise ratio in low concentrations is high because of single particle counting.

In addition to condensation techniques, the aerosol particle concentrations are often measured with electrostatic methods by first artificially charging the neutral particles. Charged particles can be classified according to their d_P by leading them to an electric field within a differential mobility analyzer (DMA). After a size selection in the electric field, the concentration of particles can be determined by measuring the current delivered by the flow of charged particles to an electrometer, or by a CPC. The limitation of electrometers is their sensitivity, whereas condensational techniques are sensitive to the chemical composition of the particles and to the smallest detectable size. Instruments that measure the mobility diameter do not yield information about whether the detected nanoparticle is a particle, cluster or a large molecule.

A limitation of the DMA is its ability to size-select only charged particles. It is necessary to bring the sample to an equilibrium

charge distribution using forced charging. In many applications, this is achieved with artificial unipolar or bipolar charging[65]. The electrical detection of clusters is a challenging task because of small concentrations, transport losses and insufficient charging efficiency of small neutral particles. Thus, electrical instruments need to be sensitive enough to distinguish the minuscule signal brought in by the clusters from the instrument background. To tackle the difficulties in the electrical techniques, high flow rates and optimized charging are used to minimize the ion diffusion losses and to increase the sensitivity to the ion concentrations. A detailed description of the different instrument types, their verification and calibration can be found in the **Supplementary Methods**.

In regional NPF, the measurement location should be chosen carefully to make the measurement representative of the whole region of interest. When comparing data from several instruments, they should be sampling from the same height and preferably close to each other. Any local pollution sources should be avoided or taken into account later in the data analysis. Exhaust gases from the instruments should be led away from the sampling site. In **Table 2**, we have summarized the properties of the main instruments used at the Hyytiälä site for observing atmospheric NPF.

To capture the initial formation of atmospheric nanoparticles and their dynamical features, one needs to consider several prerequisites. The instrumentation should fulfill requirements both on the time resolution and on the smallest detectable size. Furthermore, the instrumentation should be compatible with the spatial scale of interest. This can vary from one location to another depending on

the source area of the new particles. In regional NPF events, the spatial extent typically varies from tens to hundreds of kilometers, whereas other types of events can occur in a rather confined space. This needs to be considered when upscaling the results. The vertical extent should also be noted.

Because of diffusion losses of the small particles, the inlet and sampling lines of the instruments need to be kept as short as possible. The tube diameter should be chosen such that the aerosol flow stays laminar. However, if one insists on having a very short residence time, the flow could be turbulent. The inlet lines and connectors should be made from conductive material (preferably stainless steel) in order to avoid accumulation of static electric charge. If possible, additional bypass flows can be used to reduce diffusion losses. In front of the inlet, a rain cover or an insect net can be placed if necessary. Proper preconditioning of the aerosol is dependent on the instrument.

The measurement platform sets constraints to the time resolution needed for capturing the NPF. In regional ground-based measurements, a time resolution of 10 min is sufficient, whereas onboard aircrafts the data acquisition frequency needs to be 1 Hz or faster depending, e.g., on the cruise speed.

In terms of long-term observations, some redundancy in the measurements is beneficial to obtain reliable long-term data sets for NPF. This also provides instrumental comparison and quality assurance of the scientific findings. In particular, colocated long-term measurement activities capable of measuring both the charged clusters and the neutral pathway are important[66–70]. Data with instruments with slightly different cutoff sizes provide information that can be used in the scaling of the formation rates down

to the sizes at which the initial nucleation occurs[53]. As an example, in **Table 2**, we have listed the relevant instruments used at the SMEAR II (ref. 20) in Hyytiälä to quantify the NPF occurring in the boreal forest environment.

The timeline for instrument deployment at a field site in Hyytiälä is presented in **Figure 1**. These instruments represent a suite of devices capable of detecting the concentration and size of atmospheric nanoparticles and clusters. In addition, the atmospheric pressure interface time-of-flight (Api-TOF) mass spectrometer can be used to extract information on chemical composition of atmospheric ions[34,35]. Another emerging technique is the cluster chemical ionization mass spectrometer[36].

Special considerations for detecting sub-3-nm particles. The measurements in the sub-3-nm size range are demanding and cannot be performed with standard instrumentation. Insufficient particle detection can lead to misinterpretation of data, including the functional dependence of the particle formation rate on nucleating vapor concentrations. This was illustrated by Sipilä *et al.*[21], who showed that the measurement of nucleation rate is extremely sensitive to the capability to detect the smallest particles.

One must bear in mind that when dealing with particles in the size range of <3 nm, bulk properties (e.g., surface tension, density) do not necessarily hold and even the particle size itself cannot necessarily be unambiguously determined.

The smallest particles (i) are easily lost by diffusion during sample transport, (ii) are difficult to charge for electrical classification, (iii) are problematic for collecting representative samples for electrical detection, (iv) are present in insufficient amounts for chemical analysis and (v) require a very high supersaturation to grow to a size large enough for optical detection. Because of

these challenges in measuring sub-3-nm particles, it is ideal to use different methods to determine the concentration of particles in the range of <3 nm and their evolution in order to avoid any bias. Thus, the measurement arrangements for atmospheric NPF studies typically include complementary instruments for detecting both negative and positive ions, as well as neutral aerosol particles.

Procedure overview

Identifying atmospheric NPF from ambient measurements is performed on the basis of inspecting the measured size distribution data, usually from DMPS or ion spectrometer measurements[71,72]. The general procedure is described in Steps 1–10 of the PROCEDURE, with instrument-specific variations described in detail.

The identification and classification of regional (banana-type) NPF is typically performed 1 d at a time. This is reasonable because most NPF bursts have been observed to occur during daytime, mostly in a time window centered around noon. Instead of marking exact time periods as formation periods, the day-by-day approach allows the classification of each day as either event day or non-event day. Non-event days can be divided into either clear non-event days or the days on which some nucleation-mode particles do appear but without clear growth of particles.

TABLE 2 | Specification of various instruments used for measuring atmospheric nucleation at the Hyytiälä site.

	Size range (nm)	Type of particles	Time resolution
DMPS	3–1,000	Total	10 min
PSM (scanning)	1–1,000 (1–2 for size distribution)	Total, neutral	1 s (2 min for scanning)
CPCB	2–10	Total	1 s

NAIS	2–42	Total, neutral, ions	3–5 min			
AIS	0.9–42	Ions	5 min			
Sample flow rate (liters min^{-1})	**Approximate maintenance interval**				**Additional information**	
5	1 week				Radioactive source, butanol	
2.5	Up to 1 week				DEG, butanol/ water	
2.5–5	1 d				Butanol, water	
60	1–3 months				Corona-needle charger	
60	1–3 months				—	
BSMA	0.9–8.0	Ions	10 min	2,600	1–3 months	—

The aerosol dynamic processes ongoing in the atmosphere usually lead to a size distribution that is composed of one or more log-normally distributed modes. A regional NPF event leads to the formation of a new mode, the nucleation mode. The intensity and duration of the formation and the rapidity of the particle growth determine the evolution of this mode in time. As a result, the observed changes in this mode can be used to determine the dynamic parameters of the particle formation[24,73].

To become atmospherically relevant and observable with commonly applied instruments, the newly formed particle of about 1.5 nm in diameter needs to grow in size[33]. The rate of growth is an important dynamic parameter related to atmospheric NPF. We describe two methods[24,71,74–77] for determining the GR of freshly formed particles (Steps 6–8 of the PROCEDURE).

The formation or nucleation rate is determined as described in Step 10 of the PROCEDURE. See previous studies for more information[16,24,62,71,78]. To determine the nucleation rate, one needs to determine the condensation and coagulation sinks[24,73,79] (CS and CoagS, respectively; Step 9 in the PROCEDURE). The nucleation rate can be measured directly by instruments capable of detecting particles that are small enough (1.5 ± 0.4 nm)[16,21]. If the smallest size is larger (up to 10 nm), the nucleation rate at smaller sizes can be extrapolated using theoretical methods[25,80–82].

As references for analyzing point or line sources of particles, we can refer to studies on coastline particle formation. On the basis of NPF observations on an Atlantic coast site in Mace Head, Ireland,

Vana *et al.*[83] proposed several additional event types: apple, hump and mixed type. This event classification was later used by Yli-Juuti *et al.*[84] and Manninen *et al.*[62] when analyzing ion spectrometer measurements in various European measurement sites. The main feature of these event types is the sudden appearance of particles

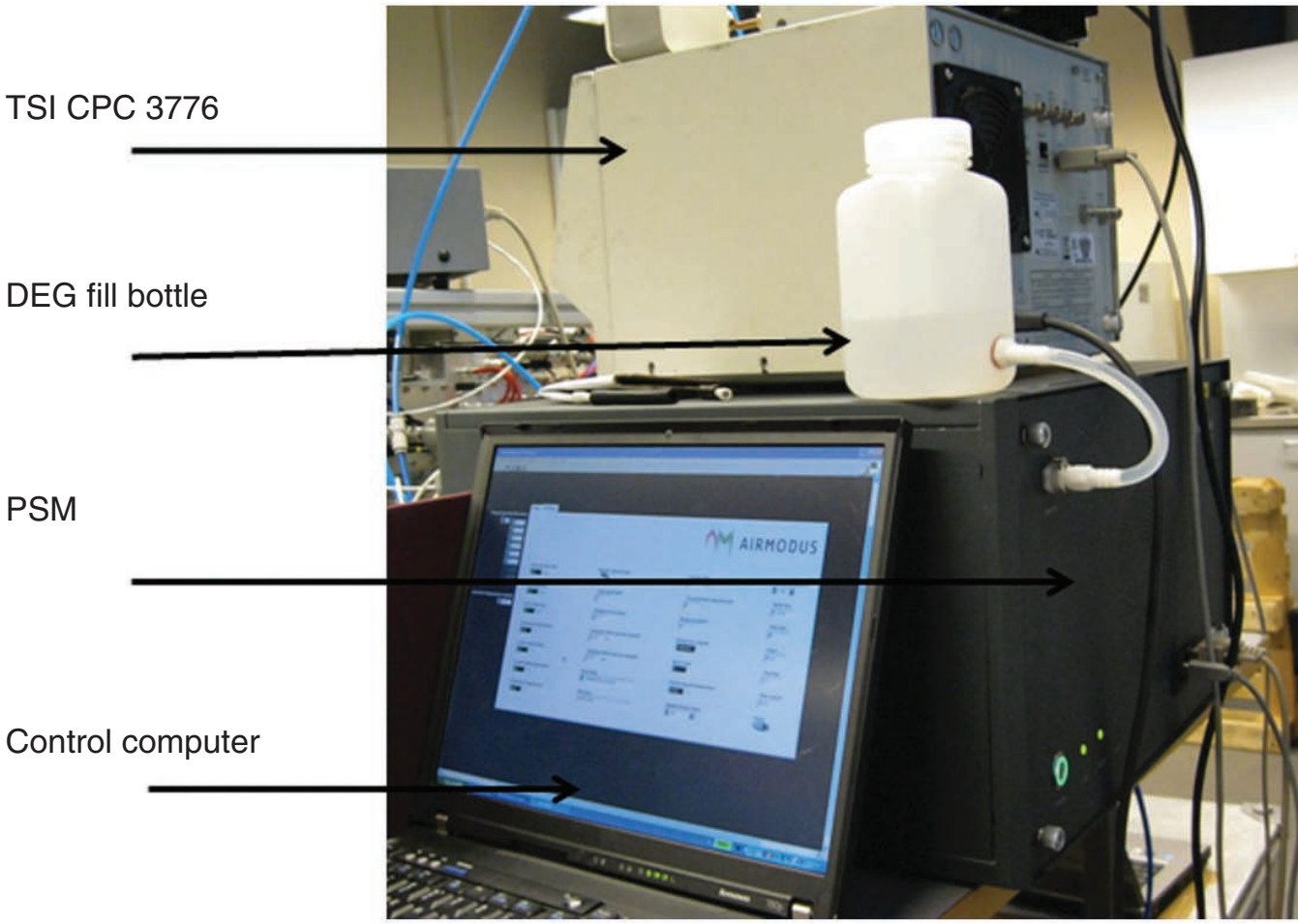

Figure 2 | The PSM A09 with the CPC 3776 (TSI).

smaller than 25 nm, but there is no clear growth observed. This is typical for a well-localized (or point-like) particle source, as all the observed new particles have grown approximately the same amount of time during the transport to the measurement location.

The rate of formation of new atmospheric particles ultimately determines the number concentration of particles that enter the atmosphere as a result of nucleation. As most of the effects of atmospheric aerosols depend on the particle number concentration, this dynamic parameter is of crucial interest. In the following procedure, we will describe the basic methodology to obtain particle formation rates especially during regional NPF events from atmospheric observations.

MATERIALS

REAGENTS

▲ **CRITICAL** The listed reagents are working fluids for the CPCs. The working fluid used depends on the exact type and model of the instruments; consult the instrument manuals for details. Also refer to corresponding material safety data sheets before use.

- 1-Butanol (CAS no. 71-36-3), reagent grade ! **CAUTION** Butanol is hazardous and flammable (health hazard 1, fire hazard 3, personal protection H).
- Isopropyl alcohol (CAS no. 67-63-0), reagent grade ! **CAUTION** It is hazardous and flammable (health hazard 2, fire hazard 3, personal protection H).

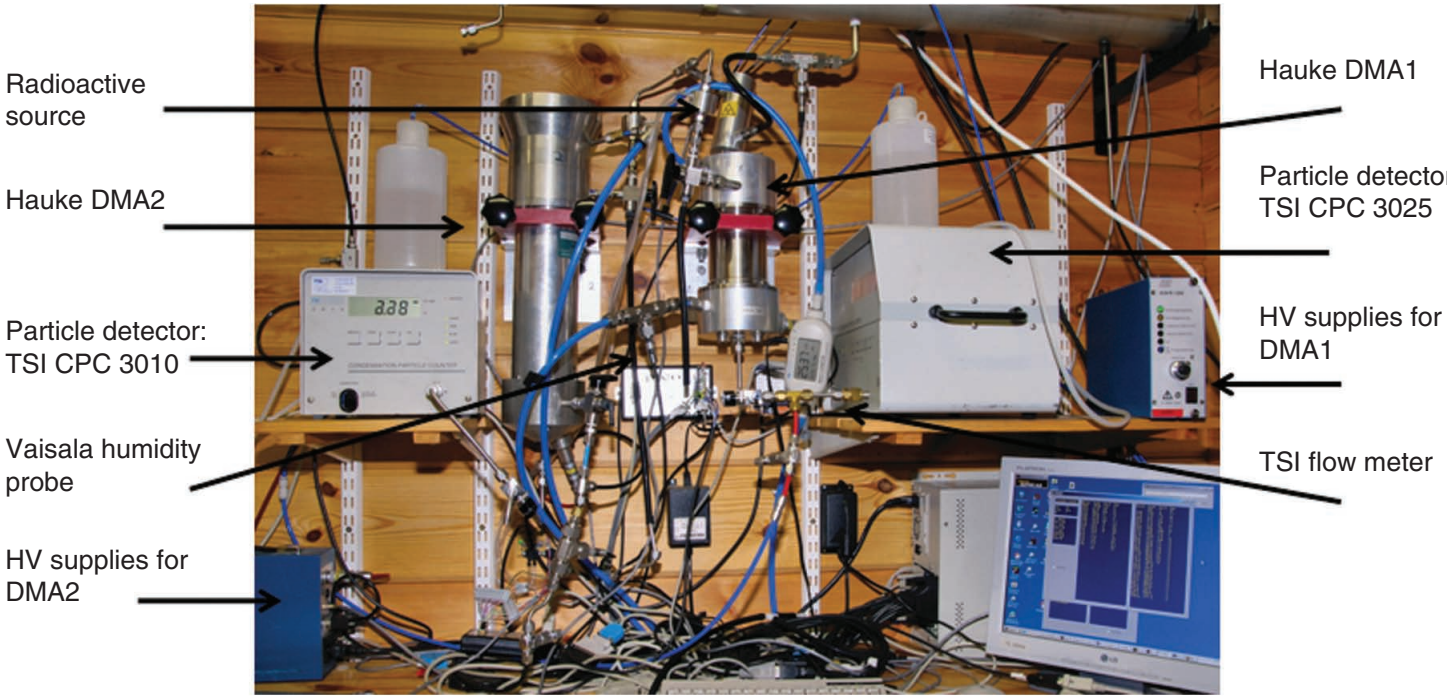

Figure 3 | The twin-DMPS system in Hyytiälä. HV, high voltage.

- DEG (CAS no. 111-46-6), reagent grade
  ! CAUTION DEG is hazardous and may be combustible at high temperatures (health hazard 1, fire hazard 1, personal protection H).
- Water (ultrapurified, from Millipore system)

EQUIPMENT

- CPC (see EQUIPMENT SETUP)
- Electrostatic particle sizers (see EQUIPMENT SETUP)

EQUIPMENT SETUP

▲ CRITICAL The instruments suitable for

determining the aerosol particle formation or nucleation rate are briefly overviewed and listed below. The exact setting of required instruments depends on the research strategy. The instruments applied in the measurements of atmospheric particle concentrations rely typically on one of the two following methods or on the combination of both: condensation

techniques or electrostatic techniques. Some operation parameters of the instruments are calibrated and some are only verified, the difference being that the calibration involves the adjustment of the device, whereas the verification only verifies the proper operation of the instrument. See the **Supplementary Methods** for more details.

Condensation particle counter A CPC with the detection efficiency in the size range of <3 nm, preferably at 1.5 nm (refs. 18, 43–47) is required. For determining particle size distribution, at least one of the following setups is needed: a suite of CPCs with slightly different cutoff sizes[85–89]; a condensation particle counter battery[53,54]; a PSM[18] (**Fig. 2**); or a PH-CPC[56–60]).

Electrostatic particle sizers The following instruments measure the size distribution of neutral particles (NAIS also measures that of charged particles): (i) DMPS[48–51] (**Fig. 3**); SMPS[52] or DEG-SMPS[47]; and (ii) NAIS[16,55] (**Fig. 4**). The following instruments measure only the size distribution of charged particles: (i) AIS[61,62]; (ii) BSMA[63] (**Fig. 5**); and (iii) SIGMA[64].

Figure 4 | The NAIS.

Figure 5 | The BSMA.

PROCEDURE

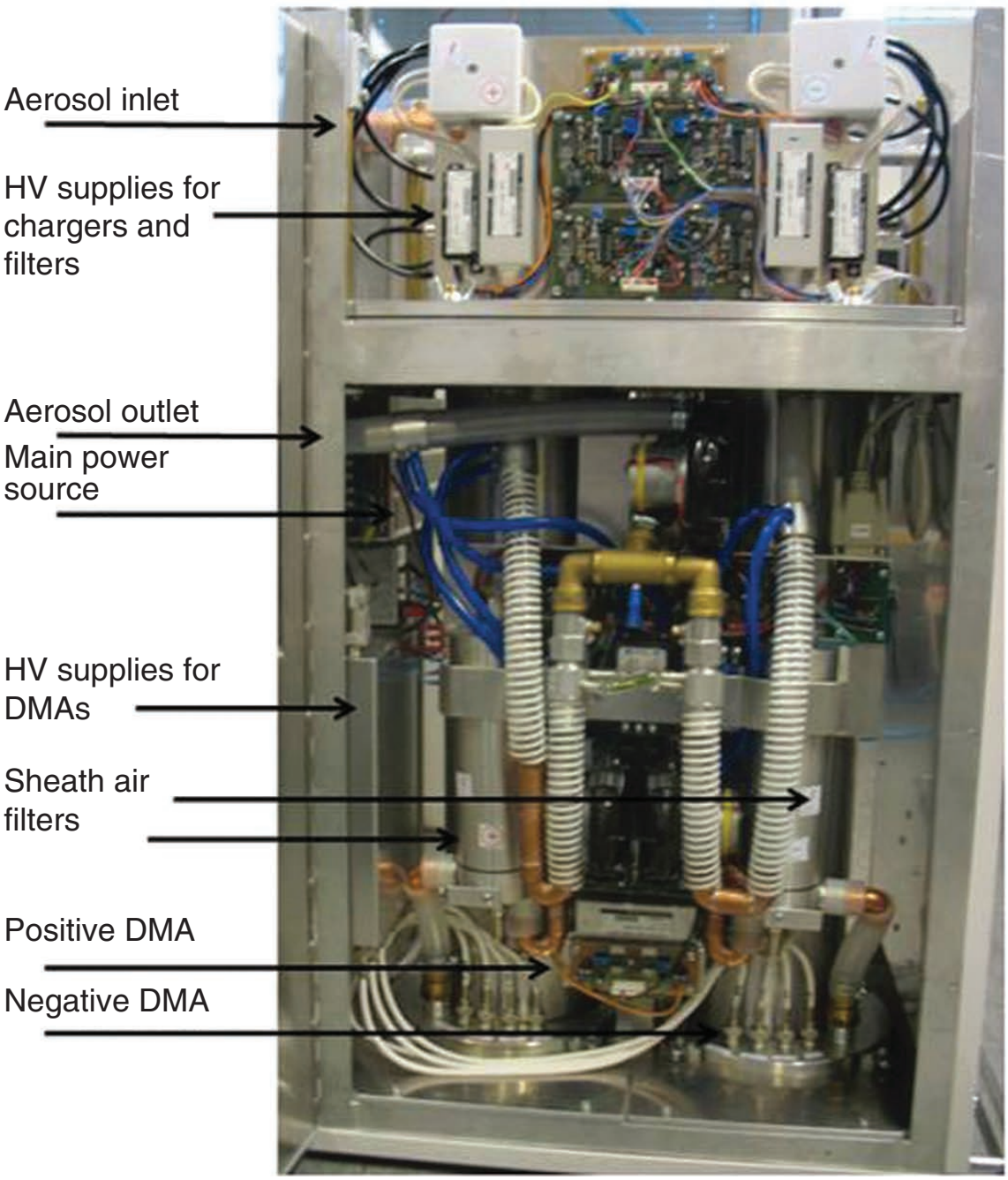
Aerosol inlet
HV supplies for chargers and filters
Aerosol outlet
Main power source
HV supplies for DMAs
Sheath air filters
Positive DMA
Negative DMA

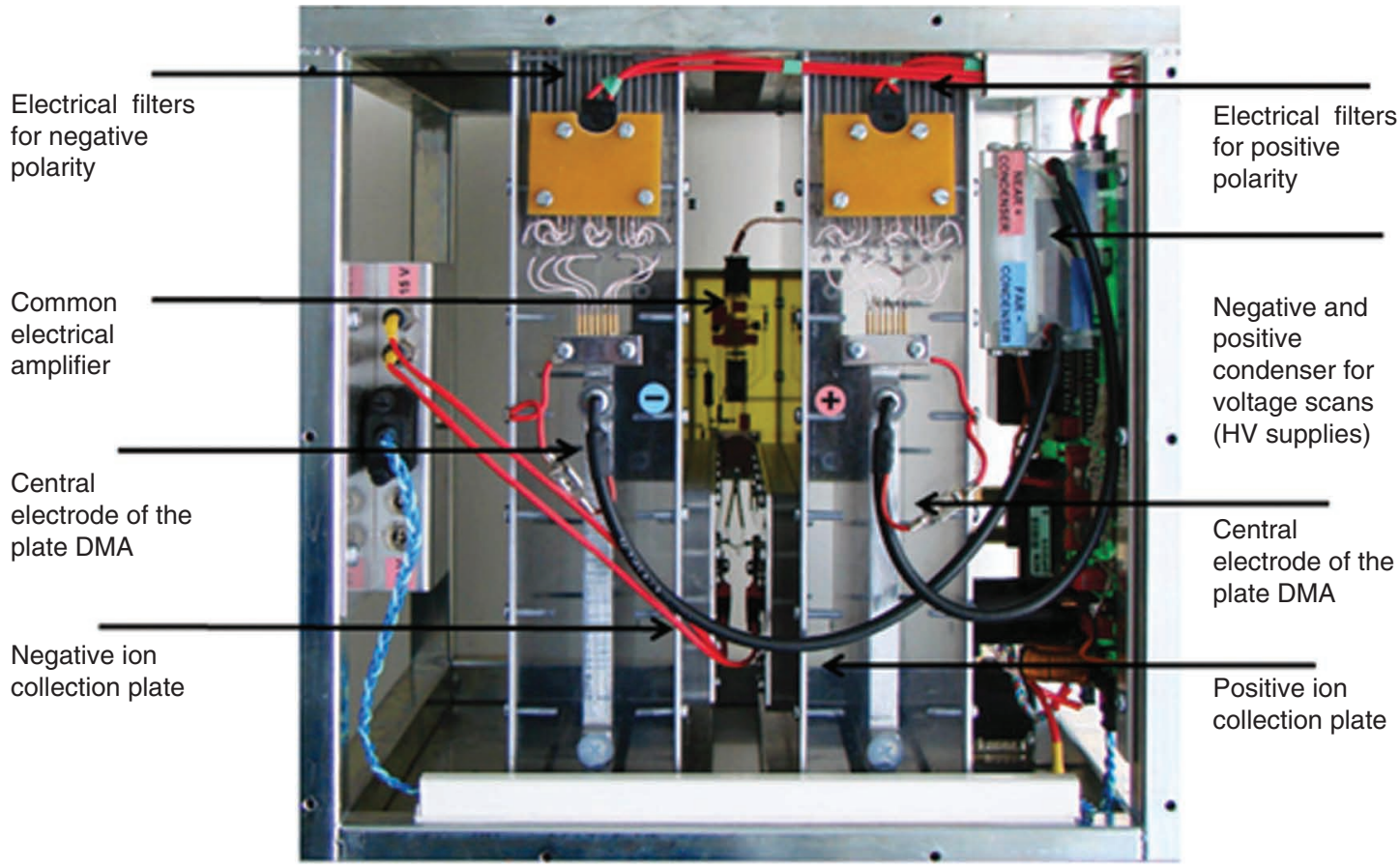

▲ **CRITICAL** It is important to carefully plan the measurement instrumentation and location by taking into account the considerations described in the INTRODUCTION before following the PROCEDURE.

Data collection ● TIMING 24 h—continuous

1| Measure the particle and/or ion number size distribution, preferably between 1 and 1,000 nm, with the instrumentation described above. The smallest detectable particle size defines the size at which the formation rate can be directly quantified (Step 10 of the PROCEDURE). In addition, instruments measuring size distribution of larger particles (e.g., DMPS, SMPS) are needed for determining the CoagS and CS (Step 9 of the PROCEDURE). Parallel measurements with ion and aerosol instrumentation enable quantification of neutral and ion-induced formation mechanisms.

Data analysis and evaluation: event analysis

▲ **CRITICAL** Data analysis and evaluation is a continuous process taking 3 h. The first step is the event analysis where one will find out the whether an NPF event has occurred or not. The main result of the event analysis is the frequency of new particle formation events.

2| Perform data inversion and verify the observations of particle or ion size distributions.

? TROUBLESHOOTING

3| Plot the particle size distributions as a function of time. The data inversion usually returns a particle number concentration density function $dN/d\ (\log_{10} d_p)$ given at a number of diameters that are logarithmically spaced. If these points vary during the day, the inverted data points can be interpolated to the same size grid. The established convention is to plot a 1-d time series of the size distributions as flat surface plots. In the surface plots, the *x* axis represents time, the *y* axis shows the particle diameter on a logarithmically spaced scale and the *z* axis, which is usually represented by

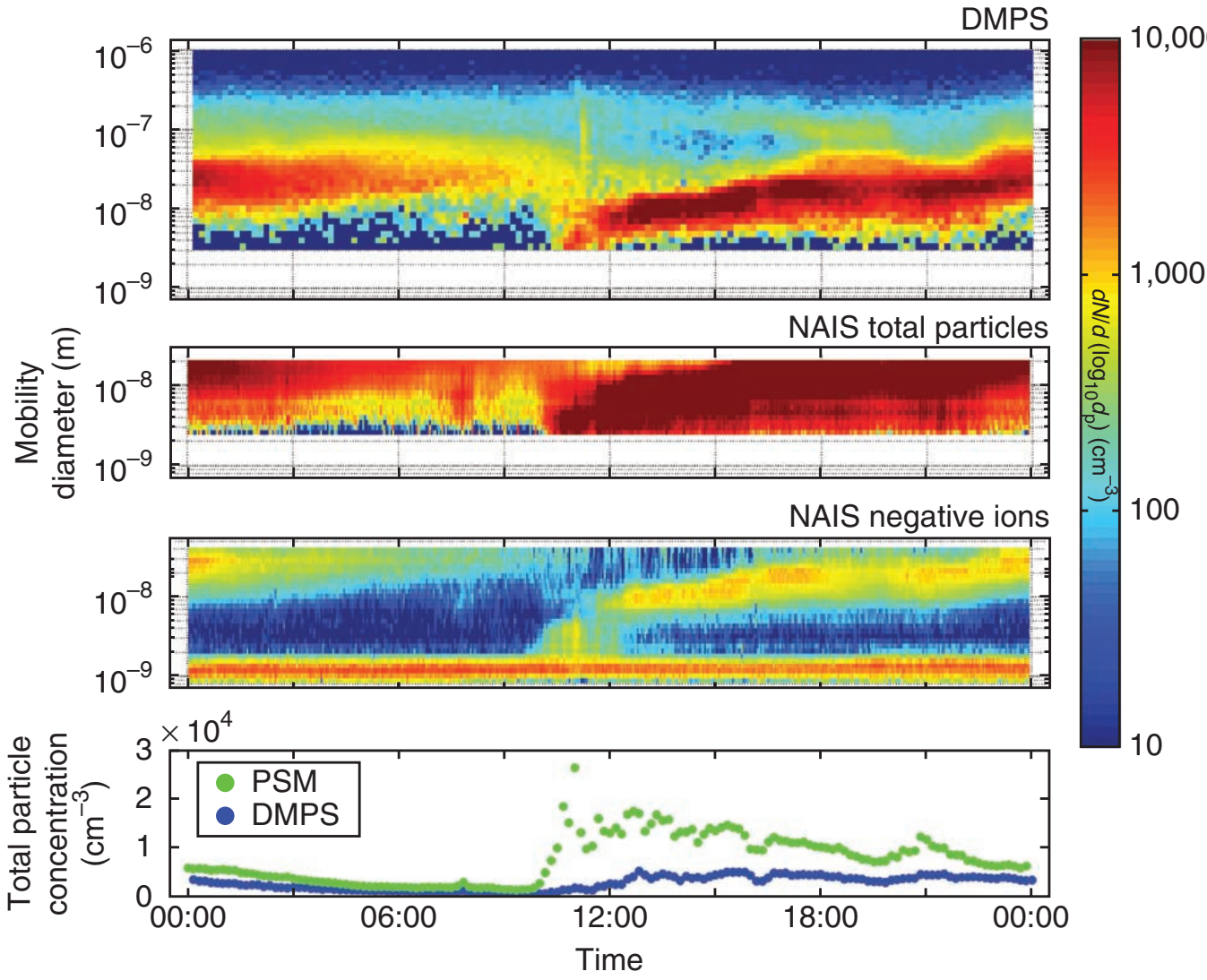

Figure 6 | New particle formation event observed in Hyytiälä on 26 March 2011. Top, the upper three images show the size distribution evolution during the day measured by DMPS, as well as NAIS in total and negative ion mode. Bottom, the total particle concentration between 3 and 1,000 nm measured by DMPS and the concentration of particles larger than 1.6 nm measured by PSM.

different colors, represents the particle number concentration density (**Fig. 6**). By convention, the concentration density is plotted on a logarithmic scale because of the high variation in the concentration density in the atmosphere.

4| Visually or automatically identify NPF events from the size distribution time series and classify days as either NPF event or non-event days. The decision-making during the event classification depends on the extent of the particle formation that one tries to identify. Conventionally, in atmospheric measurements at a fixed point, one is interested in particle formation that is occurring fairly uniformly over a geographically large area. Then the aerosol processes leading to changes in the size distribution can be considered to be independent of transport processes.

The NPF event classification is performed visually, primarily on the basis of the surface plots of the time series of the number size distributions and the time evolution of nucleation-mode particles[71,72,90,91]. All available particle, ion and cluster data should be considered simultaneously, with the emphasis on the data on the smallest particles and clusters (that is, particles of sizes close to or below 3 nm in diameter and ion and cluster measurements, whenever they are available).

The classification is based on the question 'Can we observe a particle formation signature in the observed measurements in the vicinity of the measurement point?'. If the answer is yes, the day is classified as an event day; if no, the day is classified

as a non-event day. To separate the data further, one can also distinguish a group of days as undefined, if the signature of the formation is ambiguous. An algorithm for automatic detection of particle formation is described in **Box 1**.

The features of a particle formation signature are described in the in-text table below. Owing to the heterogeneous nature of the atmosphere, varying geographical features and possible non-nucleation particle sources, the clarity of the NPF features

Box 1 | Automatic detection of regional new particle formation

To detect regional new particle formation, the monitored air masses have to stay constant over the period of interested growth range. Thus, only regional NPF events that occur during conditions of stable air masses are possible to detect. The detection is based on monitoring time evolvement of aerosol size distribution.

The detection includes the following steps:

1. Aerosol data are cleaned from noise (single exceptionally high values) by applying a three-point median filter.
2. The data are smoothed by a two-dimensional smoothing algorithm (five points in the particle size dimension and nine points in the time dimension (90 min), moving median; **Fig. 11**).
3. The aerosol number size distribution below 20 nm is considered.
4. The concentration of particles larger than 20 nm particles is subtracted from the smaller sizes.
5. Regions of positive values are marked with 1 and the others with 0. The region of data marked with 1 is called the region of interest (ROI). In the example data shown in **Figure 11**, two ROIs are found (**Fig. 12a**).
6. The 25^{th} percentile value of all particle concentrations within a ROI is calculated and set as a threshold value.
7. Revised ROI is calculated by looking for data values that are above the threshold and within a time range of 12 h from the starting moment of the initial ROI (**Fig. 12b**).

(continued)

Box 1 | (continued)

8. The revised ROIs are NPF events. If the event occurred during light hours (after sunrise and before sunset), an event can be considered as a regional NPF. **Figure 13** depicts the automatically detected event regions using this procedure.

Although identifying particle formation bursts is, in principle, simple, there are some complications that require refinements in the classification guidelines. One of the main assumptions in the analysis is that the measurement is made in a uniform air mass with the same properties for an extended period of time. Because of the turbulent nature of the atmosphere, the validity of this assumption varies. This causes fluctuations in the observed size distributions, which can make the analysis of the event properties more difficult, or even make the distinction between particle formation and transported aerosol difficult. Therefore, it was noted earlier that a classification system was needed to somehow get a measure on the amount of trust that could be placed in the derived characteristics.

in the observed size distribution varies. In particular, combustion sources nearby often cause feature 1 to be observed, and in the case of a strong or large source, feature 2 is also possible. Therefore, for regional particle formation, all three features are required for a day to be classified as an event day. If none of the features 1–3 are observed, the day is classified as a non-event day. If some but not all of features 1–3 are observed, the convention is to classify these days as undefined. The purpose of this is to remove these days from event and non-event comparisons, as one cannot be fully sure whether regional NPF is occurring.

Sometimes, both signatures of local nanoparticle sources and regional NPF can be observed, and the local source signatures can obfuscate the regional NPF signatures fully or partly. The convention is to classify these days as event days if the local signature can be clearly separated from the regional NPF signature. If doubt exists, the day is classified as undefined. The same applies if only clear local source signatures are observed: these days should be classified as non-event days.

Feature 1: increase of nucleation mode (<25 nm) particle concentration	This is a required feature. The size limit is set at 25 nm due to the possibility that nucleation occurs at some distance from the measurement point and the particles grow a few nanometers before they are being observed
Feature 2: formation of a new, distinct nucleation mode persisting for several hours	This is a feature of regional particle formation. The lack of this feature is usually a signature of particle formation processes that are not regional, such as point or line sources of nanoparticles
Feature 3: growth of the nucleation mode over several hours	The growth of particles is required for the particle formation to be observed using field instrumentation. If no growth is occurring, fresh particles would quickly be lost because of various loss processes. Therefore, the observable growth of the nucleation mode is conventionally required for a day to be classified as a regional NPF day

5| Determine the particle formation period from the event days identified in Step 4.

Determine the GR

6| The observed particle GR is defined as the rate of change in the diameter, d_p, that represents the growing particle population:

$$\mathrm{GR} = \frac{dd_p}{dt} = \frac{\Delta d_p}{\Delta t} = \frac{d_{p2} - d_{p1}}{t_2 - t_1} \quad (2)$$

where d_{p1} and d_{p2} are the representative particle diameters at times t_1 and t_2, respectively.

Depending on how the representative diameter is chosen, particle GRs can be determined from the growing nucleation mode by using (at least) two methods (e.g., options A and B below). These two methods have been extensively compared on the basis of a 7-year data set from the Hyytiälä SMEAR II station by Yli-Juuti *et al.*[77]. The GRs obtained by the two methods were observed to agree with each other, typically within a factor of 2. Both of these methods require, however, that the particle growth can be followed for several hours. Because of this, these methods are not ideal for analyzing events other than regional NPF events. Other methods are discussed in **Box 2**.

(A) Maximum-concentration method

(i) With this method[92], the representative diameter is determined as the center of the measured size bin. Define the times, t_n, when the concentration maximum reaches each size bin. Usually there are constant fluctuations and measurement noise in the particle concentrations. Locating the exact time of the peak concentration therefore needs to be done by fitting a suitable function to the concentration time series around the approximate maximum location.

Box 2 | Other methods for determining the growth rate

If the measurement setup allows the determination of the charging state of the new particle population, one can apply the method introduced by Iida *et al.*[74] to determine the growth rate. This method benefits from the fact that it does not require a well-behaving nucleation mode. Automated methods, based on analyzing changes in the whole size distribution, also exist[107,108]. The key advantage of these methods is that they automatically take into account the influence of all aerosol dynamic processes on the growth rate. Such methods should, however, be applied with care, as they are more prone to errors due to the nonisotropic aerosol field that is mostly observed in field conditions.

Measurements of ambient sulfuric acid concentration can be used to yield estimates for the growth rates of the freshly formed particles. It has been observed in several studies[23,27–30] that the concentration of new aerosol follows the concentration of sulfuric acid with a time delay. This time delay is related to the growth from the critical cluster to the detection limit, and GR can thus be determined from

$$\mathrm{GR} = \frac{d_{\mathrm{p,cutoff}} - d^*}{\Delta t} \quad (3)$$

where $d_{\mathrm{p,cutoff}}$ is the lower detection limit of the concentration measurement (e.g., CPC), d^* is the critical cluster size where the initial nucleation occurs and Δt is the time difference between the rise in the ambient sulfuric acid concentration and the concentrations of new small particles. This method is particularly useful in, for example, situations in which no detailed size distribution data exists, but measurements of sulfuric acid concentrations are available.

(ii) Plot the representative particle sizes as a function of time. An example of how this method is applied is shown in the four upper images in **Figure 7**.

? TROUBLESHOOTING

(B) Log-normal distribution function method

(i) Typical submicron atmospheric size distributions can be described by 2–4 log-normal modes[93–95]. Fit log-normal distribution functions to the measured number size distribution at each time step. Define the representative particle size for each time step as the geometric mean of the fitted distribution function, which is also the median size of the log-normal distribution. The fitting itself is usually done using least-squares minimization, with initial values for the minimization algorithm given by the user; there are also automatic size distribution fitting algorithms that use more sophisticated statistical methods to perform the fitting[96].

(ii) Plot the representative particle sizes as a function of time. An example of how this method is applied is shown in the four upper images in **Figure 8**.

? TROUBLESHOOTING

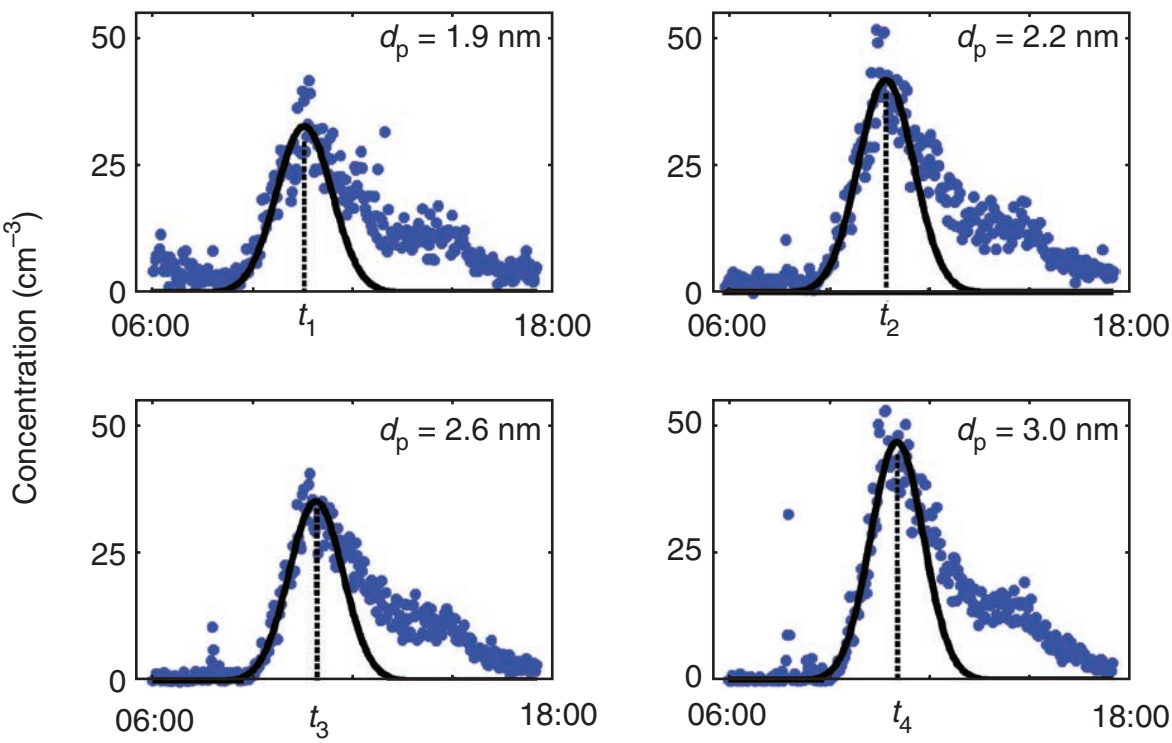

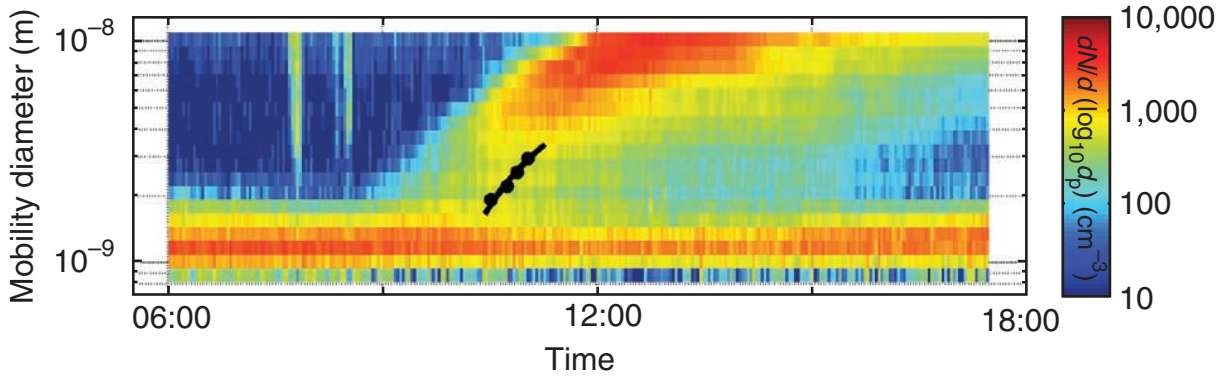

Figure 7 | Growth rate determination by the maximum-concentration method. In the top four images, particle number concentration in four size fractions is shown with blue points, and the black curves are normal distributions fitted to the area around maximum concentration. The peak times t_1, t_2, t_3 and t_4 are shown with black dots in the bottom image. Growth rate is determined by a linear least-squares fit to these points (black line).

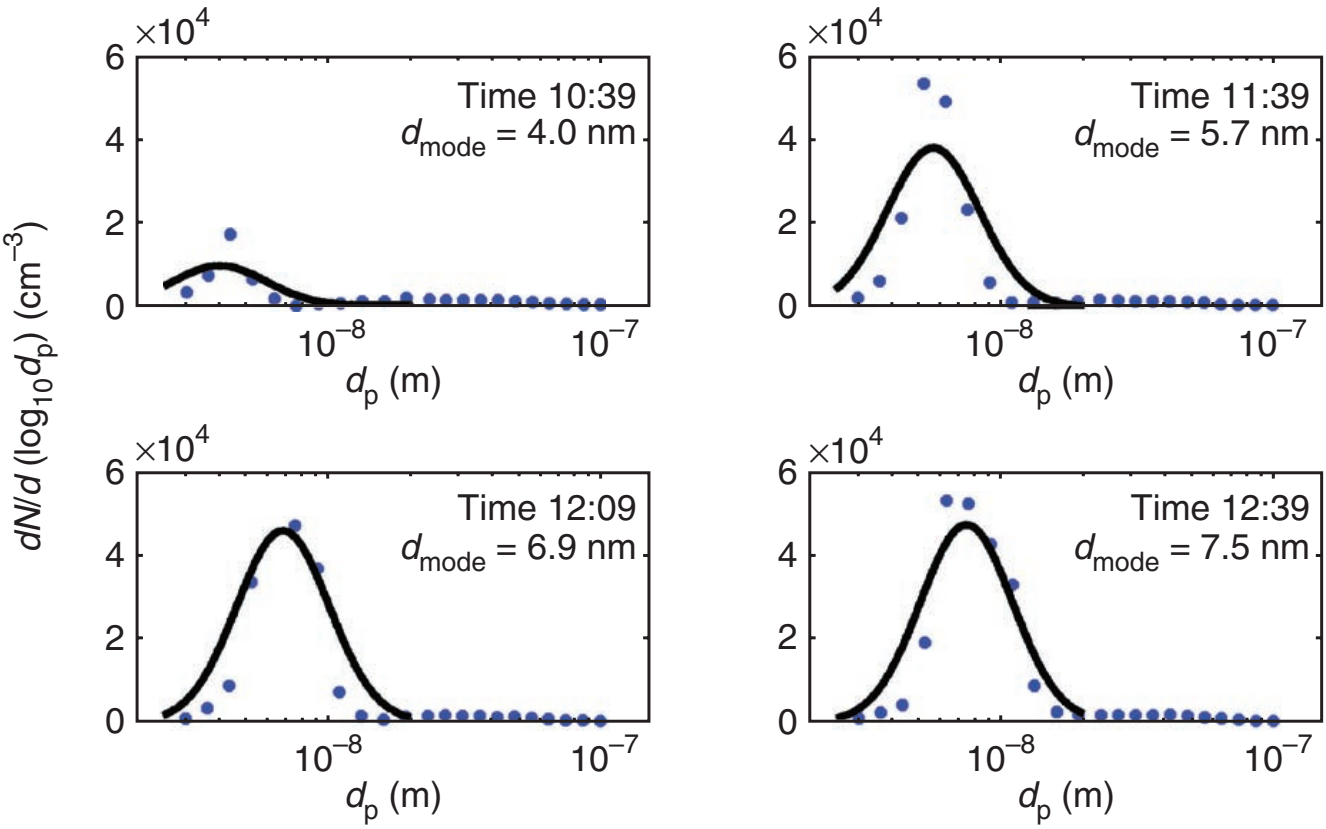

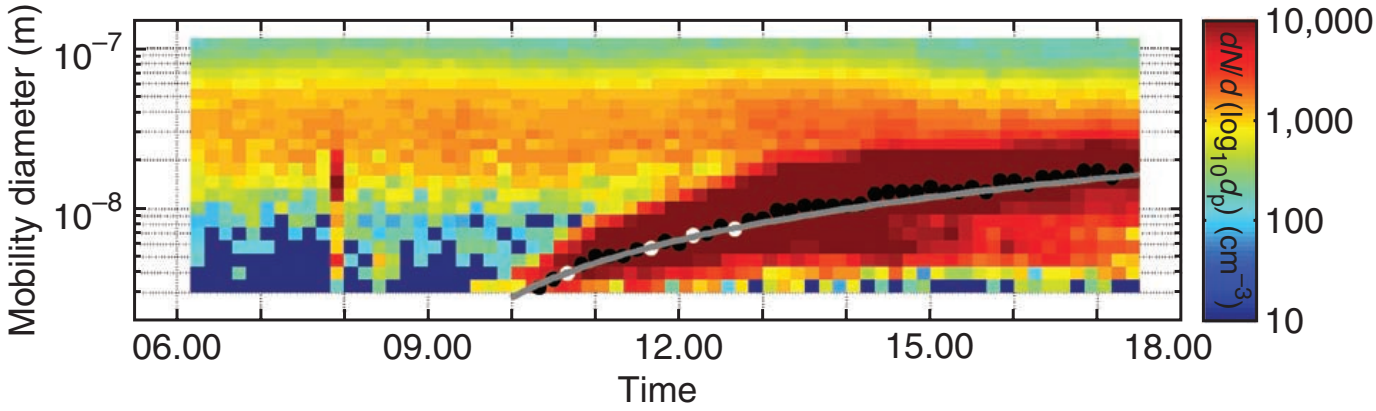

Figure 8 | Particle growth rate determined by the mode-fitting method. The top four images show particle size distributions (blue points) at times 10:39, 11:39, 12:09 and 12:39. The black curve is the fitted nucleation mode. Bottom, the geometric mean diameters of the fitted modes are shown by black dots (the modes of the top images are marked by white dots). The gray line is linear least-squares fit to these points.

7| Calculate the GR from the slope of a liner fit to data points obtained in Step 6. The determination of the slope can be done either for the whole duration of the observed particle formation event or it can be performed for selected time or size windows. In the first case, one obtains the overall GR during NPF. When using different windows, time- or size-dependent GRs can be obtained. Typical particle size windows used are <3, 3–7, 7–20 and >20 nm (ref. 62). Examples of the GR fittings to the data points determined with options A and B in Step 6 are shown in the lower images of **Figures 7** and **8**.

8| Correct for self-coagulation and coagulation scavenging. The observed GR of the representative diameter depends not only on the condensational GR of the particles in the population but also on their coagulation. As one is usually interested in the condensational GR of particles, corrections to the observed GR need to be introduced. These include the real GR due to self-coagulation of the growing particle population, and the apparent GR due to selective coagulation scavenging of growing particles by larger particles. Leppä *et al.*[76] presented simple analytical formulas to take these corrections into account. It should be noted that the coagulation scavenging correction is only needed for the log-normal particle fitting method; for the maximum-concentration method, correcting for self-coagulation is enough. Another important result of the Leppä *et al.*[76] study was that using linear normalizations of the size distribution function (dN/dd_p) with the above-mentioned methods (Step 6) gives more accurate GR estimations than the logarithmic normalizations dN/d ($\log_{10}d_p$) that have typically been used.

Calculate the size distribution–dependent particle loss parameters

9| Calculate the CoagS and the CS. The CoagS for particles with diameter d_p can be calculated from the measured size distribution[79]:

$$\mathrm{CoagS}_{d_p} = \int K\left(d_p, d_p'\right) n\left(d_p'\right) dd_p' \cong \sum_{d_p'=d_p}^{d_p'=\max} K(d_p, d_p') N_{d_p'} \tag{4}$$

where K (d_p, d_p') is the coagulation coefficient of particle sizes d_p and d_p'. The CoagS is related to the CS[24], which describes the condensing vapor sink caused by the particle population:

$$\mathrm{CS} = 4\pi D \int_0^{d_p\,\max} \beta_m(d_p') d_p' N_{d_p'} dd_p' = 4\pi D \sum_{d_p'} \beta_{m,d_p'} d_p' N_{d_p'} \tag{5}$$

where D is the diffusion coefficient of the condensing vapor, usually assumed to be sulfuric acid, and β_m represents a transition-regime correction[97],

$$\beta_m = \frac{1+Kn}{1+1.677Kn+1.333Kn^2} \tag{6}$$

defined as a function of the Knudsen number[97], $Kn = 2\lambda/d_p$. The accommodation coefficients for mass and heat transfer are assumed to be unity when calculating the value of CS. To simplify calculations, Lehtinen *et al.*[81] gave a relation linking CS and CoagS. The value of CS is conventionally calculated routinely for each size distribution (Step 1), as it can be used to obtain CoagS for varying size bins. For typical conditions at the Hyytiälä station, the relation can be approximated by

$$\mathrm{CoagS}_{d_p} = \mathrm{CS} \bullet \left(\frac{d_p}{0.71}\right)^m \tag{7}$$

where d_p is given in nm and the exponent m is about −1.6.

Determine the formation or nucleation rate

10| The time evolution of particle number concentration, N_{d_p}, in the size range [d_p, $d_p + \Delta d_p$] can be described in general terms as

$$\frac{dN_{d_p}}{dt} = \text{production} - \text{losses} = J_{d_p} - \text{losses} \tag{8}$$

The production term is the NPF rate at size d_p, denoted by J_{d_p}. The loss terms include coagulation losses due to larger aerosol particles and condensational growth out of the considered size range. Wall and other surface losses need to be considered when analyzing, for example, chamber measurement data, but in atmospheric observations such losses can usually be

neglected. In atmospheric measurements made at a fixed location, air mass dilution due to boundary layer development and other processes affecting air mass homogeneity should, in principle, be taken into account.
Calculate the neutral particle formation rate by reorganizing equation (8) and including the loss terms:

$$J_{d_p} = \frac{dN_{d_p}}{dt} + \mathrm{CoagS}_{d_p} \bullet N_{d_p} + \frac{\mathrm{GR}}{\Delta d_p} \bullet N_{d_p} + S_{\mathrm{losses}} \quad (9)$$

where CoagS_{d_p} is the CoagS of particles in the size range [d_p, $d_p + \Delta d_p$], GR is their growth rate and S_{losses} includes additional losses.

When determining the formation rate of positively (superscript +) or negatively (superscript –) charged particles, $J_{d_p}^{\pm}$, two additional terms need to be added to equation (9):

$$J_{d_p}^{\pm} = \frac{dN_{d_p}^{\pm}}{dt} + \mathrm{CoagS}_{d_p} \bullet N_{d_p}^{\pm} + \frac{\mathrm{GR}}{\Delta d_p} \bullet N_{d_p}^{\pm} + \alpha \bullet N_{d_p}^{\pm} \bullet N_{<d_p}^{\mp} - \chi \bullet N_{d_p} \bullet N_{<d_p}^{\pm} \quad (10)$$

The fourth term on the right-hand side of this equation represents ion-ion recombination and the fifth term is charging of neutral particles by smaller ions. The subscript $<d_p$ refers to all particles smaller than d_p in diameter. The ion-ion recombination coefficient α and the ion-aerosol attachment coefficient χ can be determined either from measurements or theory, and they depend in principle on particle size. Typical values used for α and χ are equal to 1.6×10^{-6} cm^3 s^{-1} and 0.01×10^{-6} cm^3 s^{-1}, respectively[98].

Calculate the true nucleation rate. It is very important to distinguish between the terms particle formation rate and nucleation rate. The formation rates are typically referred to as J_2, J_3 and so on depending on the size of the smallest observed particles. The nucleation rate is the rate at which critical clusters (i.e., clusters large enough to start growing) are being formed. As these critical clusters grow to larger sizes, coagulation and deposition scavenge certain fraction of them before they reach the detection limit of the instrument, and hence observed particle formation rates are always smaller than the true nucleation rate[80–82].

If the particle (or cluster) size distribution has been measured below 1.5 nm (e.g., by applying scanning PSM), the atmospheric nucleation rate can be determined directly by using equation (9).

If one has not measured the true atmospheric nucleation rate, J^*, that produces clusters of diameter d^*, but rather the formation rate of particles of some larger diameter d_p, termed J_{d_p}, the relationship between J^* and J_{d_p} can be estimated by taking into account the condensational growth and coagulation scavenging. Kerminen and Kulmala[80] presented a formula connecting J^* and J_{d_p}:

$$J_{d_p} = J^* \exp\left\{\gamma\left(\frac{1}{d_p} - \frac{1}{d^*}\right)\frac{\mathrm{CS}}{\mathrm{GR}_{d^*-d_p}}\right\} \quad (11)$$

Here $\mathrm{GR}_{d^*-d_p}$ is the GR of nucleated particles from d^* to d_p. The parameter γ depends on many factors but can usually be approximated by assuming it to be equal to 0.23 nm^2 m^2 h^{-1} (ref. 79).

As can be seen from equation (11), the estimate for the formation rate below the detection limit depends exponentially on two parameters that are not known from measurements: $\mathrm{GR}_{d^*-d_p}$ and d^*. These need to be estimated on the basis of existing information. According to present information, d^* is equal to 1.5 ± 0.4 nm (refs. 16,21,22). The value of $\mathrm{GR}_{d^*-d_p}$ has conventionally been approximated by the particle GR in the size window nearest to it in size space. This approximation may not be valid, as $\mathrm{GR}_{d^*-d_p}$ is influenced by the Kelvin effect, by molecular properties of the condensation process[75] and by the presence of charges[76]. Because of these factors, the observed formation rate J_{d_p} should always be reported, along with the estimations for d^* and $\mathrm{GR}_{d^*-d_p}$ used in calculating J^*. An alternative way to estimate $\mathrm{GR}_{d^*-d_p}$ is to deduce it from the time delay between the rise in sulfuric acid concentration and the rise in the concentration of newly formed particles.
The accuracy of this method is thus susceptible to processes that are difficult to quantify.

Other formulations for calculating J^* have been given in the literature[25]. Lehtinen *et al.*[81] presented a formulation that was derived using the relationship between CS and CoagS (equation (7)). For situations with high nucleating particle concentrations, leading to self-coagulation that can skew the results given by equation (11), Anttila *et al.*[82] modified this solution to include such effects.

The main approximation in equation (11) comes from the assumption of constant GR, both as a function of size and time. By analyzing computer-generated synthetic events, Korhonen *et al.*[78] found that for cases with significant size dependence in the GR and high CoagS using equation (11) may result in errors up to an order of magnitude when estimating nucleation rates from observed formation rates. With improving instrument detection efficiency, however, the use of equation (11) is becoming increasingly reliable.

? TROUBLESHOOTING

11| (Optional) After separating events from other days, classify them into quantifiable and nonquantifiable events. Quantifiable events are event days for which the retrieval of dynamic parameters (Steps 6–10) is successful. For nonquantifiable events, the retrieval failed for some reason (e.g., a sudden change of air mass). This classification should only be performed after attempting the retrieval of dynamic parameters. It is often useful, because in further analysis other supporting data such as meteorological variables and trace gas concentrations can then be studied when formation and GRs are reliably determined. This provides some insight into, e.g., the role of different vapors and processes leading to the NPF process.

? TROUBLESHOOTING

Troubleshooting advice can be found in **Table 3**.

TABLE 3 | Troubleshooting table.

Step	Problem	Solution
2	New particle formation is not observed	The initial nucleation process is not occurring at the vicinity of the measurement location. One should increase spatial coverage of measurements both in horizontal and vertical scales
		Sampled particles are lost prior observation. One should minimize sampling losses in the instrument inlets
		Instrument is not sensitive to the particles with a particular composition. One should verify response with variable particle composition and use various methods in parallel
		Instrument malfunction. One should verify instruments in the laboratory conditions against a reference instrument
		No formation is occurring because of small precursor production rates or large condensation sink
6A(ii), 6B(ii),10	Nucleation rate in the range of <3 nm and/or growth rate cannot be determined	All particles/clusters in the size range of 1.5–3.0 nm do appear at the same time. This is probably due to the fact that the initial nucleation process is not occurring at the vicinity of the measurement location. One should increase spatial coverage of measurements both in horizontal and vertical scales
		Nucleation and/or growth rate is fluctuating strongly. Consider applying longer time averaging; also assess the role of local sources in the vicinity
		Determine the lowest formation rate that can be reliably measured with the instruments. Values below this limit are due to instrumental noise. Consider also a possibility that the formation does not occur at the site
		Growth rate is unreasonably high. The NPF event is not regional one. Reanalyze the data in local/coastal point of view

● TIMING

Long-term continuous observations are needed to obtain reliable results on atmospheric NPF. The minimum measurement time period is several weeks in case of individual event studies, and 1 year for determining the seasonal frequency of NPF events[7,55,62,71,77,93,94,99–101].

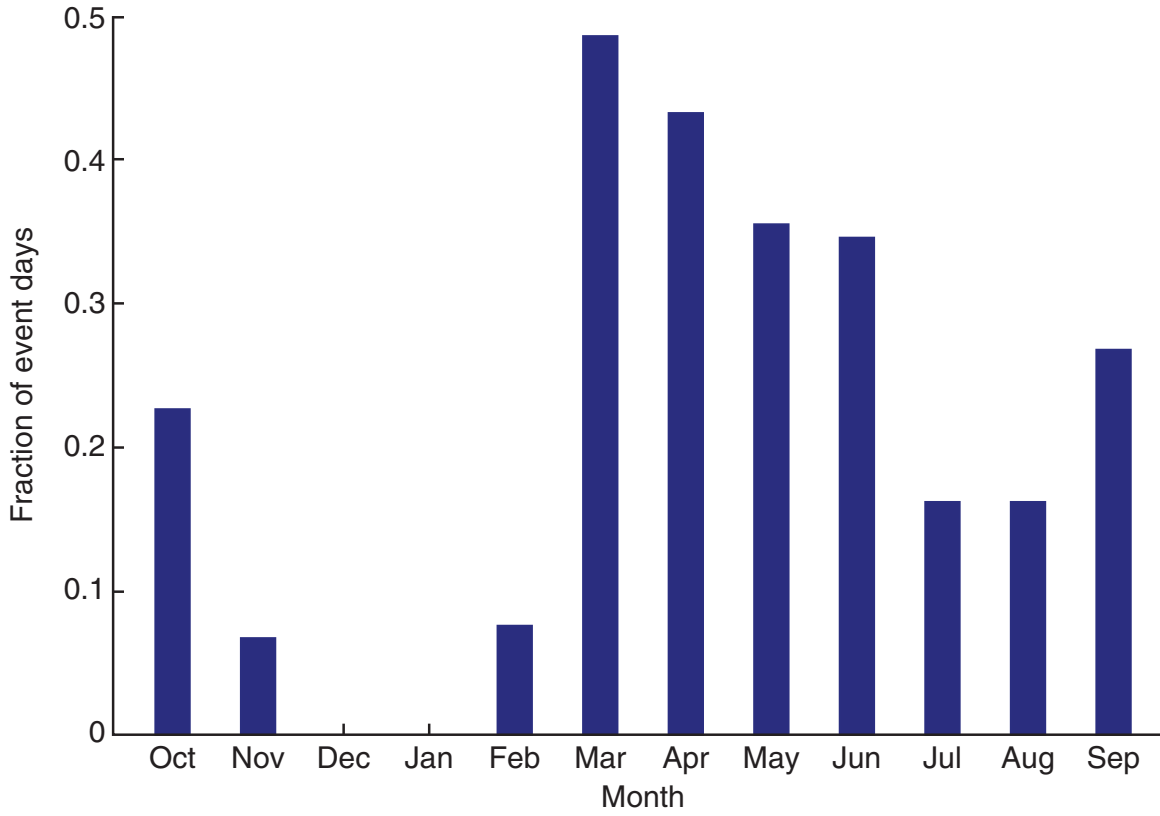

Figure 9 | Monthly fraction of days when NPF events were observed in Hyytiälä SMEAR II station between October 2010 and September 2011.

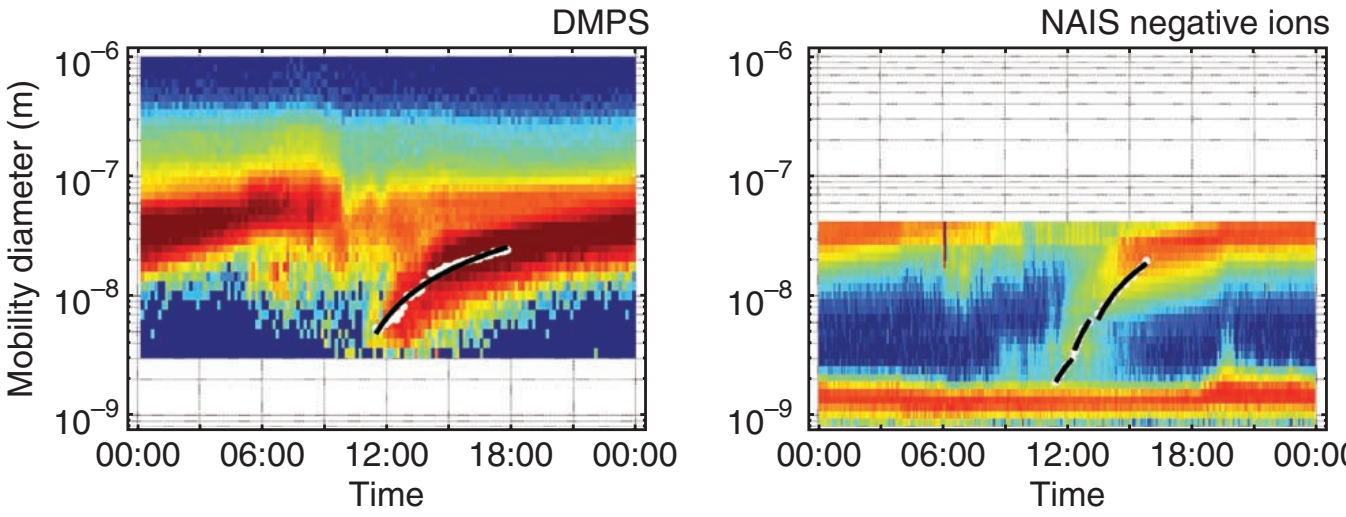

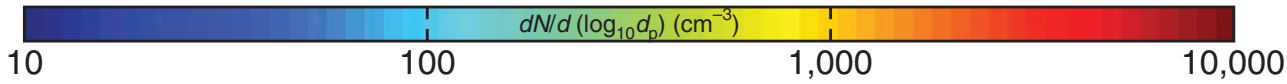

Figure 10 | NPF event on 28 April 2011 in Hyytiälä. Growth rates are determined with the two methods introduced in this protocol. Left, DMPS data and the geometric means of the fitted nucleation mode; right, negative ion spectra from NAIS with the size-bin–specific concentration maxima. Black lines are linear least-square fits. Growth rates are the slopes of these lines.

ANTICIPATED RESULTS

To illustrate atmospheric NPF, we show an example of the particle size distribution evolution during a NPF event day in **Figure 6**. During the morning hours around 10:00, a new mode—the nucleation mode—is observed to appear at 3 nm, along with an increase in the number concentration. If no anthropogenic combustion sources are nearby, the source of such small particles is usually the transformation of gaseous matter to the particle phase either by homogeneous or heterogeneous nucleation (activation), or vapor condensation onto very small undetectable clusters. This is called an NPF event[6]. The newly formed particles then grow typically for several hours until they have reached sizes of 50–100 nm. During the growth, particles coagulate with pre-existing larger particles and their number concentration is thereby reduced. A frequently observed feature taking place before a new formation event is the reduction of pre-existing particle number concentration characterized by the CS[24]. This may be the result of the growth of the planetary boundary layer after sunrise leading to apparent dilution of particle concentration. In the majority of atmospheric situations, the subsequent growth of these particles is caused by condensation of a vapor or vapors onto the particle surfaces[24,33], whereas the decline in their number concentration is mainly due to their coagulation with larger particles[26,79].

The spatial area where NPF is taking place affects the shape and the observed time evolution of the measured size distributions. If the source of new particles is a point source (e.g., a single factory), a line (e.g., a busy road) or a relatively small, confined area close to the measurement site, the shift (growth) of particles toward larger sizes cannot usually be observed. If, however, the formation is occurring over a larger area (regional NPF event), the formation can be seen in a time series of measured size distributions as a distinct shape[71] shown in **Figure 6**.

By following the PROCEDURE, we are able to find out NPF days (see **Fig. 9**) and determine the corresponding event statistics and particle growth and formation rates. As an example, we present here results of the event analysis for the Hyytiälä SMEAR II station between October 2010 and September 2011. The event classification was made on the basis of both DMPS and NAIS size distribution measurements.

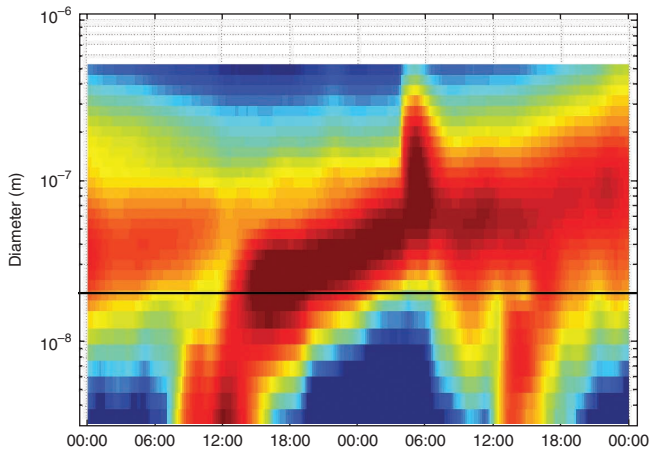

Figure 11 | Smoothed aerosol size distribution for 15–16 April 2004. Black line denotes the 20-nm limit.

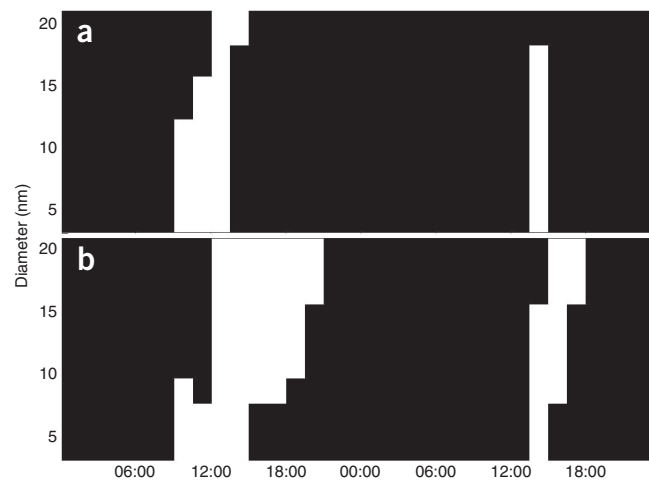

Figure 12 | Regions of interest (ROIs) for the regional NPF detection. (**a**) Highlighted regions in which particle concentration is higher than the concentration of 20-nm particles. (**b**) Highlighted regions in which the particle concentration is higher than the threshold value (25% percentile value of ROIs in **a**).

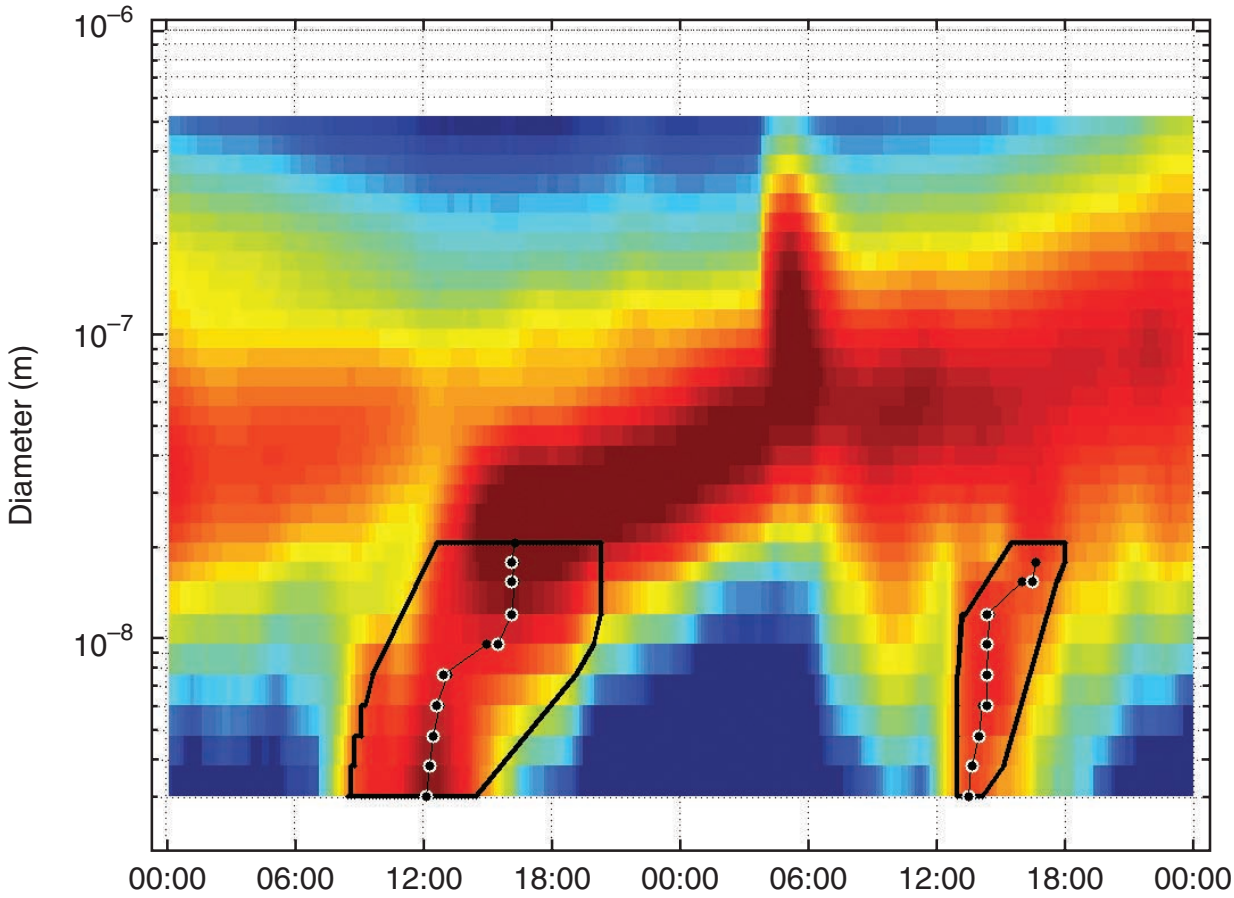

Figure 13 | Automatically detected regional NPF events. The first event starts on 15 April 2004 at 08:28:44 and the second on 16 April 2004 at 12:58:45.

NPF was observed on 78 days until the end of September. **Figure 9** shows the monthly distribution of these event days in Hyytiälä. The most frequent NPF time is in spring. In March and April 2011, almost every other day was an NPF event day. This is typical for the SMEAR II station, as can be seen from Dal Maso *et al.*[71] who presented an 8-year time series of observations at this station. This spring maximum in the occurrence of events is probably related to the start

of biogenic activity and associated emissions of various volatile organic compounds from the surrounding forest[102,103]. A second maximum in the event occurrence takes place in September. There are long-term observations from other environments that show different types of seasonal patterns with respect to event occurrence[2,100,101,104].

As more detailed results, we analyze one event day to obtain the GR as a function of size and NPF rates at 3.0, 2.0 and 1.5 nm. **Figure 10** shows the analysis of particle GR

TABLE 4 | Formation and growth rates determined for the NPF event shown in **Figure 10**.

GR_{3-25} (nm h^{-1})	3.3
$GR_{<3}$	
Tot	1.4
Neg (nm h^{-1})	1.3
Pos	1.4
GR_{3-7}	
Tot	3.9
Neg (nm h^{-1})	3.8
Pos	3.4
GR_{7-20}	

Tot	4.9
Neg (nm h^{-1})	5.2
Pos	5.0
J_3 (cm^{-3} s^{-1})	0.61
J_2	
Tot	1.1
Neg (cm^{-3} s^{-1})	0.04
Pos	0.04
$J_{1.5}$ (cm^{-3} s^{-1})	1.4

'Tot', total particle population; 'neg', negative ions; 'pos', positive ions.

during NPF event on 28 April 2011. For the DMPS data, we have used the mode-fitting method[71,96] (PROCEDURE Step 6B). A maximum of three log-normal modes were fitted to each particle number size distribution. The geometric means of the modes were plotted together with particle size distributions, and the points representing the growing nucleation mode were selected. These are the white data points in **Figure 10**. The growth is followed from 3 to 25 nm. Particle GR in this size range is obtained by a linear least-squares fit (i.e., from the slope of the black line in **Fig. 10**). From the ion spectrometer data, we are able to see the first steps of the particle formation starting from the cluster ion pool below 2 nm. The GRs of ions are determined using the maximum-concentration method (PROCEDURE Step 6A). The time of the peak concentration in each channel of the ion spectrometer is shown by the white points at the right of **Figure 10**. We have determined the GRs in three size ranges: below 3, 3–7 and 7–20 nm, as well as for the whole nucleation mode (3–25 nm). The determination of the GR can also be done automatically, as described in **Box 1** and visualized in **Figures. 11–13**.

Table 4 summarizes the GRs obtained by the two methods from DMPS and NAIS data. The GRs determined from negative and positive ions and from the total particle population do not differ significantly from each other. This is probably due to the fact that during this event the particles were quite close to their charge equilibrium (i.e., the ion population was not dominating the particle formation[76]). The GRs clearly increase as a function of particle size. The observation could be explained in two ways. First, the increase of the equilibrium vapor pressure with decreasing particle size (Kelvin effect) can lower the mass flux of condensing vapors to the smallest particles. Second, because the growth of the larger particles occurs later during the day compared with the growth of the smaller particles, ambient vapor concentrations might be different during the growth of particles in different size ranges. This would lead to an apparently changing GR as a function of the particle size.

Particle formation rates are determined at three sizes: 3, 2 and 1.5 nm. The values are given in **Table 4**. The first one corresponds to the detection limit of the DMPS and the second is typically used in ion spectrometer studies. The smallest

size is determined based on PSM and is probably very close to the true atmospheric nucleation rate. The formation rates of charged 2-nm particles account for about 7% of the total observed J_2, showing that this event was dominated by neutral nucleation. The calculated formation rates increase with decreasing cutoff size: $J_{1.5} > J_2 > J_3$. This is due to the particle losses by coagulation scavenging as the particles grow from the initial nucleated size toward larger sizes[25,79–81,105,106]. This also indicates the importance of measuring the smallest particles possible to obtain reliable atmospheric nucleation rate.

Note: Supplementary information is available in the online version of the paper.

ACKNOWLEDGMENTS Financial support from a European Research Council (ERC) Advanced grant (ATM-NUCLE, 227463); an ERC Starting grant (ATMOGAIN); Academy of Finland projects 211483, 211484 and 1118615, 139656, 251427; the Norden Top Level Research Initiative 'Cryosphere-Atmosphere Interactions in a Changing Arctic Climate' (CRAICC); and the European Union (Aerosols, Clouds and Trace gases Research InfraStructure Network (ACTRIS)) are gratefully acknowledged.

AUTHOR CONTRIBUTIONS All authors contributed to the writing and planning of the paper. M.K. and V.-M.K. were responsible for the INTRODUCTION. T.P., M.S., H.E.M., K.L., M.K. and P.P.A. were responsible for the section on 'Requirements for measuring nucleation of atmospheric aerosol particles'. With regard to the 'Procedure overview', MATERIALS, and PROCEDURE sections and associated **Supplementary Methods**, T.N., M.D.M., H.J., P.P., I.R. and A.L. were responsible for the event analysis; T.N., M.D.M., I.R., K.E.J.L. and H.J. were responsible for nanoparticle GRs; V.-M.K., K.E.J.L., T.N., K.L., M.D.M., P.P. and M.K. were responsible for nucleation and formation rates; and M.K., T.P., P.P., V.-M.K., M.S., I.R. and A.L. were responsible for the overall structure of sections. T.P., M.S. and M.K. were responsible for the TROUBLESHOOTING section. T.N., M.K., H.E.M. and K.L. were responsible for the ANTICIPATED RESULTS section.

COMPETING FINANCIAL INTERESTS The authors declare no competing financial interests.

Published online at http://www.nature.com/doifinder/10.1038/nprot.2012.091. Reprints and permissions information is available online at http://www.nature.com/reprints/index.html.

1. McMurry, P.H. & Friedlander, S.K. New particle formation in the presence of aerosol. *Atmos. Environ.* **13**, 1635–1651 (1979).

2. Kulmala, M. *et al.* Formation and growth rates of ultrafine atmospheric particles: a review of observations. *J. Aerosol Sci.* **35**, 143–176 (2004).
3. Kulmala, M. & Kerminen, V.-M. On the formation and growth of atmospheric nanoparticles. *Atmos. Res.* **90**, 132–150 (2008).
4. Weber, R.J., McMurry, P.H., Eisele, F.L. & Tanner, J. Measurement of expected nucleation precursor species and 3–500 nm diameter particles at Mauna Loa observatory, Hawaii. *J. Atmos. Sci.* **52**, 2242–2257 (1995).
5. Weber, R.J. *et al.* Measured atmospheric new particle formation rates: implications for nucleation mechanisms. *Chem. Eng. Commun.* **151**, 53–64 (1996).
6. Mäkelä, J.M. *et al.* Observations of ultrafine aerosol particle formation and growth in boreal forest. *Geophys. Res. Lett.* **24**, 1219–1222 (1997).
7. Dal Maso, M. *et al.* Aerosol size distribution measurements at four Nordic field stations: identification, analysis and trajectory analysis of new particle formation bursts. *Tellus B.* **59**, 350–361 (2007).
8. Hussein, T. *et al.* Time span and spatial scale of regional new particle formation events over Finland and Southern Sweden. *Atmos. Chem. Phys.* **9**, 4699–4716 (2009).
9. O'Dowd, C.D. *et al.* A dedicated study of New Particle Formation and Fate in the Coastal Environment (PARFORCE): overview of objectives and achievements. *J. Geophys. Res.* **107**, 8108 (2002).
10. Wen, J., Zhao, Y. & Wexler, A.S. Marine particle nucleation: observation at Bodega Bay, California. *J. Geophys. Res.* **111**, D08207 (2006).
11. Spracklen, D.V. *et al.* The contribution of boundary layer nucleation events to total particle number concentrations on regional and global scales. *Atmos. Chem. Phys.* **6**, 5631–5648 (2006).
12. Yu, F. *et al.* Spatial distributions of particle number concentrations in the global troposphere: simulations, observations and implications for nucleation mechanisms. *J. Geophys. Res.* **115**, D17205 (2010).
13. Merikanto, J., Spracklen, D.V., Mann, G.W., Pickering, S.J. & Carslaw, K.S. Impact of nucleation on global CCN. *Atmos. Chem. Phys.* **9**, 8601–8616 (2009).
14. Kazil, J. *et al.* Aerosol nucleation and its role for clouds and Earth's radiative forcing in the aerosol-climate model ECHAM5-HAM. *Atmos. Chem. Phys.* **10**, 10733–10752 (2010).
15. Makkonen, R. *et al.* Air pollution control and decreasing new particle formation lead to strong climate warming. *Atmos. Chem. Phys.* **12**, 1515–1524 (2012).
16. Kulmala, M. *et al.* Towards direct measurement of atmospheric nucleation. *Science* **318**, 89–92 (2007).

17. Jiang, J. *et al.* First measurements of neutral atmospheric cluster and 1–2 nm particle number size distributions during nucleation events. *Aerosol. Sci. Technol.* **45**, ii–v (2011).
18. Vanhanen, J. *et al.* Particle size magnifier for nano-CN detection. *Aerosol. Sci. Technol.* **45**, 533–542 (2011).
19. Kulmala, M. *et al.* Atmospheric data over a solar cycle: no connection between galactic cosmic rays and new particle formation. *Atmos. Chem. Phys.* **10**, 1885–1898 (2010).
20. Hari, P. & Kulmala, M. Station for Measuring Ecocystem—Atmosphere Relations (SMEAR II). *Boreal Environ. Res.* **10**, 315–322 (2005).
21. Sipilä, M. *et al.* The role of sulfuric acid in atmospheric nucleation. *Science* **327**, 1243–1246 (2010).
22. Kirkby, J. *et al.* The role of sulfuric acid, ammonia and galactic cosmic rays in atmospheric aerosol nucleation. *Nature* **476**, 429–433 (2011).
23. Weber, R.J. *et al.* Measurements of new particle formation and ultrafine particle growth rates at a clean continental site. *J. Geophys. Res.* **102**, 4375–4386 (1997).
24. Kulmala, M. *et al.* On the formation, growth and composition of nucleation mode particles. *Tellus B* **53**, 479–490 (2001).
25. McMurry, P.H. *et al.* A criterion for new particle formation in the sulfur-rich Atlanta atmosphere. *J. Geophys. Res.* **110**, D22S02 (2005).
26. Stolzenburg, M.R. *et al.* Growth rates of freshly nucleated atmospheric particles in Atlanta. *J. Geophys. Res.* **110**, D22S05 (2005).
27. Sihto, S.-L. *et al.* Atmospheric sulphuric acid and aerosol formation: implications from atmospheric measurements for nucleation and early growth mechanisms. *Atmos. Chem. Phys.* **6**, 4079–4091 (2006).
28. Riipinen, I. *et al.* Connections between atmospheric sulphuric acid and new particle formation during QUEST III–IV campaigns in Heidelberg and Hyytiälä. *Atmos. Chem. Phys.* **7**, 1899–1914 (2007).
29. Nieminen, T. *et al.* Connection of sulphuric acid to nucleation in Boreal forest. *Environ. Sci. Technol.* **43**, 4715–4721 (2009).
30. Petäjä, T. *et al.* Sulfuric acid and OH concentrations in a boreal forest site. *Atmos. Chem. Phys.* **9**, 7435–7448 (2009).
31. Metzger, A. *et al.* Evidence for the role of organics in aerosol particle formation under atmospheric conditions. *Proc. Natl. Acad. Sci. USA* **107**, 6646–6651 (2010).
32. Paasonen, P. *et al.* On the roles of sulphuric acid and low-volatility organic

vapours in the initial steps of atmospheric new particle formation. *Atmos. Chem. Phys.* **10**, 11223–11242 (2010).
33. Riipinen, I. *et al.* Organic condensation: a vital link connecting atmospheric nucleation to aerosol climate forcing. *Atmos. Chem. Phys.* **11**, 3865–3878 (2011).
34. Junninen, H. *et al.* A high-resolution mass spectrometer to measure atmospheric ion composition. *Atmos. Meas. Tech.* **3**, 1039–1053 (2010).
35. Ehn, M. *et al.* Composition and temporal behavior of ambient ions in the boreal forest. *Atmos. Chem. Phys.* **10**, 8513–8530 (2010).
36. Zhao, J., Eisele, F.L., Titcombe, M., Kuang, C. & McMurry, P.H. Chemical ionization mass spectrometric measurements of atmospheric neutral clusters using cluster-CIMS. *J. Geophys. Res.* **115**, D08205 (2010).
37. Jokinen, T. *et al.* Atmospheric sulphuric acid and neutral cluster measurements using CI-APi-TOF. *Atmos. Chem. Phys.* **12**, 4117–4125 (2011).
38. Hinds, W.C. *Aerosol Technology* (John Wiley & Sons, 1999).
39. Seinfeld, J.H. & Pandis, S.N. *Atmospheric Chemistry and Physics—From Air Pollution to Climate Change* (Wiley-Interscience, 2006).
40. Tammet, H. Size and mobility of nanometer particles, clusters and ions. *J. Aerosol Sci.* **26**, 459–475 (1995).

41. Ku, B.K. & de la Mora, J.F. Relation between electrical mobility, mass, and size for nanodrops 1–6.5 nm in diameter in air. *Aerosol Sci. Technol.* **43**, 241–249 (2009).
42. Ehn, M. *et al.* Comparing mobility and mass measurements of atmospheric small ions. *Aerosol Sci. Technol.* **45**, 522–532 (2011).
43. Stolzenburg, M. & McMurry, P. An ultrafine aerosol condensation nucleus counter. *Aerosol Sci. Technol.* **14**, 48–65 (1991).
44. McMurry, P.H. The history of CPCs. *Aerosol Sci. Technol.* **33**, 297–322 (2000).
45. Kulmala, M., Lehtinen, K.E.J., Laakso, L., Mordas, G. & Hämeri, K. On the

existence of neutral atmospheric clusters. *Boreal Environ. Res.* **10**, 79–87 (2005a).
46. Iida, K., Stolzenburg, M.R. & McMurry, P.H. Effect of working fluid on sub-2 nm particle detection with a laminar flow ultrafine condensation particle counter. *Aerosol Sci. Technol.* **43**, 81–96 (2009).
47. Jiang, J., Chen, M., Kuang, C., Attoui, M. & McMurry, P.H. Electrical mobility spectrometer using diethylene glycol condensation particle counter for measurement of aerosol size distributions down to 1 nm. *Aerosol Sci. Technol.* **45**, 510–521 (2011).
48. Hoppel, W.A. Determination of the aerosol size distribution from the mobility distribution of the charged fraction of aerosols. *J. Aerosol Sci.* **9**, 41–54 (1978).
49. Stolzenburg, M.R. An Ultrafine Aerosol Size distribution system, Ph.D. thesis, University of Minnesota, Minneapolis, Minnesota, USA (1988).
50. Aalto, P.P. *et al.* Physical characterization of aerosol particles during nucleation events. *Tellus B* **53**, 344–358 (2001).
51. Wiedensohler, A. *et al.* Particle mobility size spectrometers: harmonization of technical standards and data structure to facilitate high quality long-term observations of atmospheric particle number size distributions. *Atmos. Meas. Tech.* **3**, 5521–5587 (2010).
52. Wang, S.C. & Flagan, R.C. Scanning electrical mobility spectrometer. *Aerosol Sci. Technol.* **13**, 230–240 (1990).
53. Kulmala, M. *et al.* The Condensation Particle Counter Battery (CPCB): a new tool to investigate the activation properties of nanoparticles. *J. Aerosol Sci.* **38**, 289–304 (2007).
54. Riipinen, I. *et al.* Applying the Condensation Particle Counter Battery (CPCB) to study the water-affinity of freshly-formed 2–9 nm particles in boreal forest. *Atmos. Chem. Phys.* **9**, 3317–3330 (2009).
55. Manninen, H.E. *et al.* Long-term field measurements of charged and neutral clusters using Neutral cluster and Air Ion Spectrometer (NAIS). *Boreal Environ. Res.* **14**, 591–605 (2009).
56. Saros, M., Weber, R.J., Marti, J. & McMurry, P.H. Ultra fine aerosol measurement using a condensation nucleus counter with pulse height analysis. *Aerosol Sci. Technol.* **25**, 200–213 (1996).
57. Dick, W.D., McMurry, P.H., Weber, R.J. & Quant, R. White-light detection for nanoparticle sizing with the TSI ultrafine condensation particle counter. *J. Nanoparticle Res.* **2**, 85–90 (2000).
58. O'Dowd, C.D., Aalto, P., Hämeri, K., Kulmala, M. & Hoffmann, T. Aerosol formation: atmospheric particles from organic vapours. *Nature* **416**, 497–498 (2002).
59. Sipilä, M. *et al.* Applicability of condensation particle counters to measure atmospheric clusters. *Atmos. Chem. Phys.* **8**, 4049–4060 (2008).
60. Sipilä, M. *et al.* Laboratory verification of PHCPC's ability to monitor

atmospheric sub-3 nm clusters. *Aerosol Sci. Technol.* **43**, 126–135 (2009).
61. Mirme, A. *et al.* A wide-range multi-channel air ion spectrometer. *Boreal Environ. Res.* **12**, 247–264 (2007).
62. Manninen, H.E. *et al.* EUCAARI ion spectrometer measurements at 12 European sites—analysis of new particle formation events. *Atmos. Chem. Phys.* **10**, 7907–7927 (2010).
63. Tammet, H. Continuous scanning of the mobility and size distribution of charged clusters and nanometer particles in atmospheric air and the Balanced Scanning Mobility Analyzer BSMA. *Atmos. Res.* **82**, 523–535 (2006).
64. Tammet, H. Symmetric inclined grid mobility analyzer for the measurement of charged clusters and fine nanoparticles in atmospheric air. *Aerosol Sci. Technol.* **45**, 468–479 (2011).
65. Flagan, R.C. History of electrical aerosol measurements. *Aerosol Sci. Technol.* **28**, 301–380 (1998).
66. Eisele, F.L. *et al.* Negative atmospheric ions and their potential role in ion-induced nucleation. *J. Geophys. Res.* **111**, D04305 (2006).
67. Iida, K. *et al.* Contribution of ion-induced nucleation to new particle formation: methodology and its application to atmospheric observations in Boulder, Colorado. *J. Geophys. Res.* **111**, D23201 (2006).
68. Laakso, L. *et al.* Detecting charging state of ultra-fine particles: instrumental development and ambient measurements. *Atmos. Chem. Phys.* **7**, 1333–1345 (2007).

69. Gagne, S., Laakso, L., Petäjä, T., Kerminen, V.-M. & Kulmala, M. Analysis of one year of Ion-DMPS data from the SMEAR II station, Finland. *Tellus B* **60**, 318–329 (2008).
70. Hirsikko, A. *et al.* Atmospheric ions and nucleation: a review of observations. *Atmos. Chem. Phys.* **11**, 767–798 (2011).
71. Dal Maso, M. *et al.* Formation and growth of fresh atmospheric aerosols: eight years of aerosol size distribution data from SMEAR II, Hyytiälä, Finland. *Boreal Env. Res.* **10**, 323–336 (2005).
72. Hirsikko, A. *et al.* Identification and classification of the formation of intermediate ions measured in boreal forest. *Atmos. Chem. Phys.* **7**, 201–210 (2007).
73. DalMaso, M. *et al.* Condensation and coagulation sinks and formation of

nucleation mode particles in coastal and boreal forest boundary layers. *J. Geophys. Res.* **107**, 8097 (2002).
74. Iida, K., Stolzenburg, M.R., McMurry, P.H. & Smith, J.N. Estimating nanoparticle growth rates from size-dependent charged fractions: analysis of new particle formation events in Mexico City. *J. Geophys. Res.* **113**, D05207 (2008).
75. Nieminen, T., Lehtinen, K.E.J. & Kulmala, M. Sub-10 nm particle growth by vapor condensation: effects of vapour molecule size and particle thermal speed. *Atmos. Chem. Phys.* **10**, 9773–9779 (2010).
76. Leppä, J., Anttila, T., Kerminen, V.-M., Kulmala, M. & Lehtinen, K.E.J. Atmospheric new particle formation: real and apparent growth of neutral and charged particles. *Atmos. Chem. Phys.* **11**, 4939–4955 (2011).
77. Yli-Juuti, T. *et al.* Nucleation mode growth rates in Hyytiälä during 2003–2009: variation with particle size, season, data analysis method and ambient conditions. *Atmos. Chem. Phys.* **11**, 12865–12886 (2011).
78. Korhonen, H., Sihto, S.-L., Kerminen, V.M. & Lehtinen, K.E.J. Evaluation of the accuracy of analysis tools for atmospheric new particle formation. *Atmos. Chem. Phys.* **11**, 3051–3066 (2011).
79. Kerminen, V.-M., Pirjola, L. & Kulmala, M. How significantly does coagulation scavenging limit atmospheric particle production. *J. Geophys. Res.* **106**, 24119–24125 (2001).
80. Kerminen, V.-M. & Kulmala, M. Analytical formulae connecting the 'real' and the 'apparent' nucleation rate and the nuclei number concentration for atmospheric nucleation events. *J. Aerosol. Sci.* **33**, 609–622 (2002).
81. Lehtinen, K.E.J., Dal Maso, M., Kulmala, M. & Kerminen, V.-M. Estimating nucleation rates from apparent particle formation rates and vice versa: revised formulation of the Kerminen–Kulmala equation. *J. Aerosol. Sci.* **38**, 988–994 (2007).
82. Anttila, T., Kerminen, V.-M. & Lehtinen, K.E.J. Parameterizing the formation rate of new particles: the effect of self-coagulation. *J. Aerosol. Sci.* **41**, 621–632 (2010).
83. Vana, M. *et al.* Characteristic features of air ions at Mace Head on the west coast of Ireland. *Atmos. Res.* **90**, 278–286 (2008).
84. Yli-Juuti, T. *et al.* Characteristics of new particle formation events and cluster ions at K-Pustzta, Hungary. *Boreal Environ. Res.* **14**, 683–698 (2009).
85. Schröder, F. & Ström, J. Aircraft measurements of submicrometer aerosol particles (>7 nm) in the midlatitude free troposphere and tropopause region. *Atmos. Res.* **44**, 333–356 (1997).
86. Brock, C.A. *et al.* Ultrafine particle size distributions measured in aircraft exhaust plumes. *J. Geophys. Res.* **105**, 26555–26567 (2000).
87. Feldpausch, P., Fiebig, M., Fritzsche, L. & Petzold, A. Measurement of ultrafine aerosol size distributions by a combination of diffusion screen separators and condensation particle counters. *J. Aerosol. Sci.* **37**, 577–597 (2006).
88. Hermann, M. *et al.* Submicrometer aerosol particle distributions in the

upper troposphere over the mid-latitude North Atlantic: results from the third route of 'CARIBIC'. *Tellus B* **60**, 106–117 (2008).
89. O'Dowd, C.D. *et al.* Airborne measurements of nucleation mode particles II: boreal forest nucleation events. *Atmos. Chem. Phys.* **9**, 937–944 (2009).
90. Kulmala, M. *et al.* On the growth of nucleation mode particles: source rates of condensable vapour in polluted and clean environments. *Atmos. Chem. Phys.* **5**, 409–416 (2005).
91. Buenrostro Mazon, S. *et al.* Classifying previously undefined days from eleven years of aerosol-particle-size distribution data from the SMEAR II station, Hyytiälä, Finland. *Atmos. Chem. Phys.* **9**, 667–676 (2009).
92. Lehtinen, K.E.J. & Kulmala, M. A model for particle formation and growth in the atmosphere with molecular resolution in size. *Atmos. Chem. Phys.* **3**, 251–257 (2002).
93. Mäkelä, J.M., Koponen, I.K., Aalto, P. & Kulmala, M. One-year data of submicron size modes of tropospheric background aerosol in Southern Finland. *J. Aerosol Sci.* **31**, 595–611 (2000).
94. Birmili, W., Wiedensohler, A., Heintzenberg, J. & Lehmann, K. Atmospheric particle number size distribution in central Europe: statistical relations to air masses and meteorology. *J. Geophys. Res.* **106**, 32005–32018 (2001).

---

95. Hoppel, W.A., Frick, G.M., Fitzgerald, J. & Larson, R.E. Marine boundary-layer measurements of new particle formation and the effects non-precipitating clouds have on aerosol size distribution. *J. Geophys. Res.* **99**, 14443–14459 (1994).
96. Hussein, T. *et al.* Evaluation of an automatic algorithm for fitting the particle number distributions. *Boreal Environ. Res.* **10**, 337–355 (2005).
97. Fuchs, N.A. & Sutugin, A.G. High-dispersed aerosols in topics. in *Current Aerosol Research* Vol. 2 (eds. Hidy, G.M. & Brock, J.R.) 1–60 (Pergamon, 1971).
98. Tammet, H. & Kulmala, M. Simulation tool for atmospheric aerosol nucleation bursts. *J. Aerosol. Sci.* **36**, 173–196 (2005).
99. Birmili, W. *et al.* The Hohenpeissenberg aerosol formation experiment (HAFEX): a long-term study including size-resolved aerosol, H_2SO_4, OH, and monoterpenes measurements. *Atmos. Chem. Phys.* **3**, 361–376 (2003).
100. Wu, Z. *et al.* New particle formation in Beijing, China: statistical analysis of a 1-year dataset. *J. Geophys. Res.* **112**, D09209 (2007).
101. Asmi, E. *et al.* Secondary new particle formation in Northern Finland Pallas site between the years 2000 and 2010. *Atmos. Chem. Phys.* **11**, 12959–12972 (2011).

102. Kulmala, M. *et al.* A new feedback mechanism linking forests, aerosols, and climate. *Atmos. Chem. Phys.* **4**, 557–562 (2004).
103. Dal Maso, M., Hari, P. & Kulmala, M. Spring recovery of photosynthesis and atmospheric particle formation. *Boreal Environ. Res.* **14**, 711–721

(2009).
104. Hamed, A. *et al.* Nucleation and growth of new particles in Po Valley, Italy. *Atmos. Chem. Phys.* **7**, 355–376 (2007).
105. Kerminen, V.-M., Lehtinen, K.E.J., Anttila, T. & Kulmala, M. Dynamics of atmospheric nucleation mode particles: a timescale analysis. *Tellus B* **56**, 135–146 (2004).
106. Pierce, J.R. & Adams, P.J. Efficiency of cloud condensation nuclei formation from ultrafine particles. *Atmos. Chem. Phys.* **7**, 1367–1379 (2007).
107. Lehtinen, K.E.J., Rannik, Ü., Petäjä, T., Kulmala, M. & Hari, P. Nucleation rate and vapor concentration estimations using a least-squares aerosol dynamics method. *J. Geophys. Res.* **109**, D21209 (2004).
108. Verheggen, B. & Mozurkewich, M. An inverse modeling procedure to determine particle growth and nucleation rates from measured aerosol size distributions. *Atmos. Chem. Phys.* **6**, 2927–2942 (2006).